

FINAL REPORT

Geophysical Imaging for Investigating the Delivery
and Distribution of Amendments in the Heterogeneous
Subsurface of the F.E. Warren AFB

ESTCP Project ER-200834

December 2012

Bob Kelley
ARS Technologies

Susan Hubbard
Jonathan Ajo-Franklin
John Peterson
Yuxin Wu
Erika Gasperikova
Lawrence Berkeley National Laboratory

Belinda Butler-Veytia
Veronica Shannon
ERM

Ron Coringrato
URS Corporation

This document has been cleared for public release



REPORT DOCUMENTATION PAGE

*Form Approved
OMB No. 0704-0188*

The public reporting burden for this collection of information is estimated to average 1 hour per response, including the time for reviewing instructions, searching existing data sources, gathering and maintaining the data needed, and completing and reviewing the collection of information. Send comments regarding this burden estimate or any other aspect of this collection of information, including suggestions for reducing the burden, to the Department of Defense, Executive Services and Communications Directorate (0704-0188). Respondents should be aware that notwithstanding any other provision of law, no person shall be subject to any penalty for failing to comply with a collection of information if it does not display a currently valid OMB control number.

PLEASE DO NOT RETURN YOUR FORM TO THE ABOVE ORGANIZATION.

1. REPORT DATE (DD-MM-YYYY)		2. REPORT TYPE		3. DATES COVERED (From - To)	
4. TITLE AND SUBTITLE				5a. CONTRACT NUMBER	
				5b. GRANT NUMBER	
				5c. PROGRAM ELEMENT NUMBER	
6. AUTHOR(S)				5d. PROJECT NUMBER	
				5e. TASK NUMBER	
				5f. WORK UNIT NUMBER	
7. PERFORMING ORGANIZATION NAME(S) AND ADDRESS(ES)				8. PERFORMING ORGANIZATION REPORT NUMBER	
9. SPONSORING/MONITORING AGENCY NAME(S) AND ADDRESS(ES)				10. SPONSOR/MONITOR'S ACRONYM(S)	
				11. SPONSOR/MONITOR'S REPORT NUMBER(S)	
12. DISTRIBUTION/AVAILABILITY STATEMENT					
13. SUPPLEMENTARY NOTES					
14. ABSTRACT					
15. SUBJECT TERMS					
16. SECURITY CLASSIFICATION OF:			17. LIMITATION OF ABSTRACT	18. NUMBER OF PAGES	19a. NAME OF RESPONSIBLE PERSON
a. REPORT	b. ABSTRACT	c. THIS PAGE			19b. TELEPHONE NUMBER (Include area code)

TABLE OF CONTENTS

1	SECTION 1 INTRODUCTION	4
1.1	Background	4
1.2	Objectives of the Demonstration	5
1.3	Regulatory Drivers	5
2	SECTION 2 TECHNOLOGY	7
2.1	Technology Description	8
2.1.1	Seismic Methods	8
2.1.2	Electrical Resistivity Method	10
2.1.3	Geophysical Data Inversion, Interpretation, and Assessment	10
2.2	Advantages and Limitations of the Technology	11
3	SECTION 3 PERFORMANCE OBJECTIVES	13
4	SECTION 4 SITE DESCRIPTION	16
4.1	Site Location	17
4.2	Site Hydrogeology	17
4.3	Contaminant Distribution	19
5	SECTION 5 TEST DESIGN	21
5.1	Conceptual Experimental Design	21
5.2	Baseline Field Characterization Activities	21
5.2.1	Plume E Field Investigation	22
5.2.2	Pilot Study Site Selection, Development, and Baseline Geophysical and Groundwater Characterization	22
5.3	Pilot Study	25
5.3.1	Phase 1 – Site Preparation Activities	25
5.3.2	Phase 2 – Fracturing and HRC [®] Emplacement Activities	25
5.3.2.1	Fracture Initiation Borehole Drilling	25
5.3.2.2	Fracture Propagation	25
5.3.2.3	Injection Well Installation and Completion	26
5.3.3	Phase 3 – Performance Monitoring Activities	26
5.3.3.1	Groundwater Monitoring	26
5.3.3.2	Post-Fracture Geophysical Monitoring	26

5.3.4	Phase 4 – Demobilization Activities.....	29
5.4	Interpretation and Validation	29
5.4.1	Groundwater Monitoring	29
5.4.2	Geophysical Monitoring	29
5.4.3	Confirmation Soil Boring Drilling and Core Analysis	34
5.4.4	Geophysical Data Interpretation	36
6	SECTION 6 PERFORMANCE ASSESSMENT	38
6.1	Quantitative Performance Objectives.....	38
6.1.1	Quantitative Objective #1	38
6.1.2	Quantitative Objective #2	38
6.1.3	Quantitative Objective #3	38
6.1.4	Quantitative Objective #4	40
6.2	Qualitative Performance Objectives.....	40
6.2.1	Qualitative Objective #1	41
6.2.2	Qualitative Objective #2	41
6.2.3	Qualitative Objective #3	41
6.2.4	Qualitative Objective #4	41
7	SECTION 7 COST ASSESSMENT.....	43
7.1	Cost Model	43
7.2	Cost Drivers.....	45
7.3	Cost Analysis.....	45
8	SECTION 8 IMPLEMENTATION ISSUES	48
9	SECTION 9 REFERENCES	49

List of Figures

Figure 1. Conceptual Fracture and Amendment Distribution.....	5
Figure 2. Data Acquisition Modes	8
Figure 3. Continuous Active Source Seismic Monitoring (CASSM) Method Geometry	9
Figure 4. F.E. Warren Air Force Base Site Location.....	16
Figure 5. Spill Site 7 and Plume E within Zone D at F.E. Warren Air Force Base.....	16
Figure 6. Plume E Intermediate Groundwater Trichloroethene Concentration Contours	19
Figure 7. Plume E Pilot Study Site	20
Figure 8. Laboratory Setup and Team Members Jonathan Ajo-Franklin and Yuxin Wu.....	22
Figure 9. Pilot Study Layout.....	23
Figure 10. Examples of ERT Data.....	24
Figure 11. Pilot Study at FEW.....	27
Figure 12. Wellhead Pressure Log.....	30
Figure 13. Results of the Integrated ML-Continuous Active Seismic Monitoring Inversion Process.....	31
Figure 14. Change in Seismic Velocity.	31
Figure 15. Relative Resolution of Seismic Methods.	32
Figure 16. Changes in Electrical Resistivity Using 2D ERT.....	33
Figure 17. Changes in Electrical Resistivity Using a 3D ERT Grid.....	33
Figure 18. Total Organic Carbon in Soils 6 inches Above and Below the Fracture (Soil bore SB03).....	35
Figure 19. Geophysical Estimation of Fracture Extension	36
Figure 20. Interpreted Fracture and Amendment Distributions.....	37

List of Tables

Table 1. Performance Objectives.....	13
Table 2. Pilot Test Performance Groundwater Parameters and Laboratory Analyses	24
Table 3. Groundwater Sample Collection Summary	28
Table 4. Geophysical Acquisition Times.....	28
Table 5. Summary of Geophysical Method Performance.....	39
Table 6. Performance Evaluation: Scenario 1.....	40
Table 7. Performance Evaluation: Scenario 2.....	40
Table 8. Cost Model.....	44
Table 9. Cost-Benefit Analysis: Scenario 1	46
Table 10. Cost-Benefit Analysis: Scenario 2.....	46

List of Appendices

- Appendix A Phase I Laboratory Experiments Summary
- Appendix B Geophysical Well Coordinates
- Appendix C Groundwater Performance Monitoring
- Appendix D Soil Boring Observations
- Appendix E Description of S-wave Source Experiments

LIST OF ACRONYMS

1D	one-dimensional
2D	two-dimensional
3D	three-dimensional
µg/L	micrograms per liter
µS/cm	micro-Siemens per centimeter
bgs	below ground surface
CERCLA	Comprehensive Environmental Response, Compensation, and Liability Act
CASSM	continuous active source seismic monitoring
<i>cis</i> -1,2-DCE	<i>cis</i> -1,2-dichloroethene
CO ₂	carbon dioxide
COC	constituent of concern
DCE	dichloroethene
DoD	Department of Defense
EAGL	Environmental and Applied Geophysics Laboratory
EC	electrical conductivity
EPA	United States Environmental Protection Agency
ERT	electrical resistivity tomography
ESTCP	Environmental Security Technology Certification Program
FEW	F.E. Warren Air Force Base
ft	feet
HRC [®]	Hydrogen Release Compound
Hz	hertz
ISCO	<i>in situ</i> chemical oxidation
LBNL	Lawrence Berkeley National Laboratory
m	meter
m/s	meters per second
MCL	maximum contaminant level
mg/L	milligrams per liter
MNA	monitored natural attenuation
ORP	oxidation reduction potential
ppb	parts per billion
psig	pounds per square inch gage

P-wave	primary-wave
RA	remedial action
RAO	Remedial Action Objective
RI	Remedial Investigation
ROD	Record of Decision
ROI	Radius of Influence
S-wave	secondary or shear wave
SS7	Spill Site 7
TCE	trichloroethene
TDS	total dissolved solids
TIC	tentatively identified compound
TOC	total organic carbon
<i>trans</i> -1,2-DCE	<i>trans</i> -1,2,-dichloroethene
VOC	volatile organic compound
VFA	volatile fatty acid
WDEQ	Wyoming Department of Environmental Quality

ACKNOWLEDGMENTS

The authors would like to thank Mr. John Wright, Chief of Environmental Restoration at F.E. Warren Air Force Base, for his support in providing the test site for this demonstration project.

EXECUTIVE SUMMARY

Engineered *in situ* treatment processes, such as *in situ* bioremediation, are being employed at many Department of Defense (DoD) installations to remediate contaminants such as volatile organic compounds (VOCs) in soil and groundwater. Many of these treatment processes involve the addition of biological and/or chemical amendments into subsurface aquifers. Several delivery techniques have been developed to facilitate and increase subsurface contact between treatment materials and contaminants, including hydraulic fracturing. Although fracture-based delivery strategies are being used to increase subsurface distribution of delivered treatment materials (i.e., amendments) within tight formations, demonstrating the actual achieved distribution using conventional borehole drilling methods can be ineffective, cost prohibitive, and accompanied by high uncertainty. In particular, emplaced fractures may lead to complicated three-dimensional (3D) geometries which can be difficult to characterize using one-dimensional (1D) (e.g., wellbore) sampling approaches. This study focused on improving our ability to develop conceptual amendment delivery models for *in situ* bioremediation and is based on the premise that geophysical imaging of amendment emplacement via hydraulic fracturing can reduce uncertainty in design and performance monitoring phases, thereby increasing efficacy and cost effectiveness of the remedial treatment.

Objectives of the Demonstration

The objectives of this Environmental Security Technology Certification Program (ESTCP) study were to (1) assess the utility of time-lapse geophysical methods for monitoring fracture development and the ability of fractures to distribute the remedial amendment, and (2) use that information together with conventional soil core and groundwater monitoring data to quantify the cost-benefit of using geophysical methods to develop an optimal delivery strategy prior to full-scale remedial action. Spill Site 7 (SS7), the location of a trichloroethene (TCE) plume at F.E. Warren Air Force Base (FEW), was used for comparison of the fracturing results for this demonstration. A remedial action (RA) involving hydraulic fracturing and *in situ* bioremediation was conducted at SS7 in 2009. A particular benefit of using SS7 as a comparison for this demonstration is that an average radius of influence (ROI) has been estimated for SS7 using conventional (wellbore-based) approaches and full-scale RA costs have been documented. Therefore, the ROI can be used to assess the potential cost-benefit of using geophysical imaging technologies for field scale implementation.

Technology Description

This study involved *in situ* bioremediation via hydraulic fracturing and the use of geophysical imaging to monitor fracture emplacement and amendment distribution. Seismic and electrical monitoring methods were the primary techniques selected for this study based on a conceptual model of geophysical detection limits of fracture and remediation processes. Laboratory studies were first conducted to confirm the conceptual models. Then a pilot study was conducted at SS7 to introduce the amendment (Hydrogen Release Compound® [HRC®]) with guar and proppant into the subsurface using hydraulic fracturing. Time-lapse electrical resistivity tomography (ERT) and seismic datasets were acquired before, during, and after fracture emplacement using both surface and crosshole-based configurations. Several seismic methods were tested, including continuous active source seismic monitoring (CASSM), which was the first-of-kind deployment for remediation monitoring. Other traditional datasets (such as groundwater contaminant

concentrations, drilling pressure and injection monitoring, surface displacement and tilt meter measurements, and drill-back validation holes) were collected and used to constrain and validate the interpretation of geophysical measurements in terms of fracture and associated system responses.

Demonstration Results

The seismic and electrical monitoring methods were found to be extremely useful in imaging fracture propagation and amendment distribution during the study. In particular, crosshole high frequency and CASSM seismic data were useful for quantifying the number and distribution of emplaced fractures, while the crosshole electrical data provided information about the distribution of amendments within and away from the fractures. A novel orbital S-wave crosswell source was also tested but technical limitations encountered during processing limited the utility of the datasets (see Appendix E). Analysis of the geophysical results, both individually and in combination, was performed to determine the size of the area impacted by the fractures. After 1 year of post-fracture monitoring, quarterly geophysics datasets indicated a minimum fracture ROI of 9 meters (m) (29.5 feet [ft]) with a 0.3 m (1.0 ft) vertical impact zone and an amendment distribution ROI of 5.2 m (17 ft) with a 0.8 m (2.5 ft) vertical zone distribution. The geophysical imaging also led to an updated conceptual model of fracture and amendment emplacement for the site. For example, the geophysical data suggested that the fractures and distributed amendment did not emanate radially from the fracture initiation point but were offset; the fracture radius was larger than expected, but the amendment distribution radius was smaller. Additionally, the geophysics confirmed that fractures cannot always be successfully emplaced in the subsurface, as was expected based on drilling indications.

The geophysically-obtained ROIs were used for subsequent cost-benefit analysis. To evaluate the performance, the observed ROIs were compared to a standard design ROI of 6.1 m (20 ft), which was borrowed from the analogue SS7 site at FEW. The cost-benefit analysis suggest that use of geophysical methods could lead to a 20% reduction in fracture initiation points when compared to the standard design, meeting one of the key technical objectives for this study. Future deployment of similar geophysically-based fracture assessments could follow a similar series of steps (figure below); (a) a pilot fracture installation with imaging, (b) determination of geophysically-informed fracture ROI (both vertical & lateral), (c) design of full-scale fracture treatment using determined fracture ROI constraints.

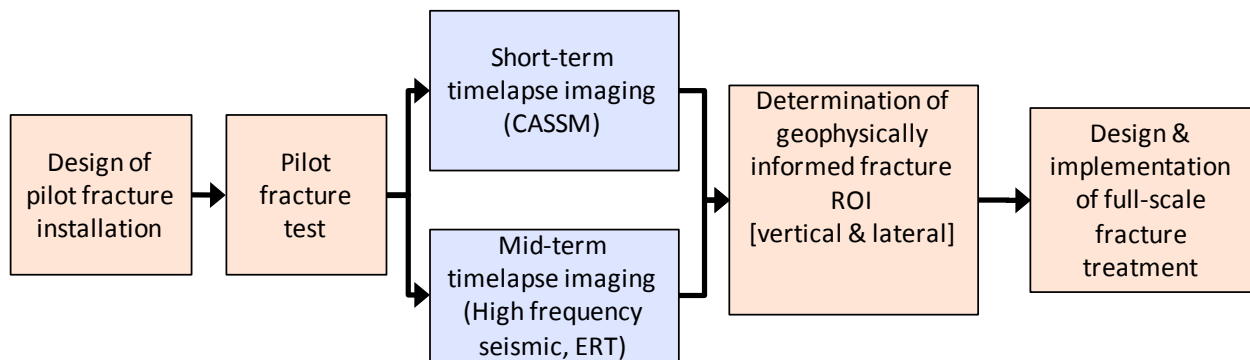


Figure 1 : Using geophysics for designing fracture remediation projects.

Implementation Issues

Several issues could potentially impact the use of geophysical data to provide high-quality data needed to design a full-scale remedial action. The first issue is the thoughtful design of the pilot study site, which should take into consideration the propagation characteristics of the different geophysical signals, the expected fracture distribution, and the costs of drilling wellbores for geophysical data acquisition. Our study found that we could estimate with high confidence the fracture and amendment distribution where wellbore placement resulted in good geophysical signal coverage, but that our certainty was low where geophysical coverage was poor or absent. Another consideration is the role of heterogeneity on fracture propagation characteristics. Our study was designed to test and image induced fracture characteristics in two different lithologies. The study illustrated that we were unsuccessful at installing fractures in one of the lithologies. Although these results highlight the value of geophysical monitoring for understanding fracture distribution as a function of heterogeneity, it emphasizes the need to also consider the geology carefully during pilot study and full-scale design of fracture-based treatment. Finally, procurement of the CASSM geophysical method also presents an implementation issue. The CASSM system was developed at Lawrence Berkeley National Laboratory (LBNL) and is not commercially available unlike the other geophysical methods tested. However, the fabrication of the CASSM system is not onerous and it could be built in the future by geophysical service providers.

SECTION 1 – INTRODUCTION

1.1 Background

Engineered *in situ* treatment processes (such as *in situ* bioremediation) are being employed at many Department of Defense (DoD) installations to remediate contaminants such as volatile organic compounds (VOCs) in soil and groundwater. Many of these treatment processes involve the addition of biological and/or chemical amendments into subsurface aquifers. These amendments facilitate reactions that degrade or destroy contaminants, converting them into innocuous compounds, such as carbon dioxide and water, which are nontoxic to humans and ecological systems. The efficacy of these *in situ* treatment processes greatly depends upon the ability to deliver amendment materials to the target contaminants. Cost of implementation and success of treatment amendment delivery is directly tied to the selected delivery strategy and the site's hydrogeological heterogeneity. Several delivery techniques have been developed to facilitate and increase subsurface contact between treatment materials and target contaminants, including hydraulic and pneumatic fracturing.

Although fracture based delivery strategies are being used to increase subsurface distribution of delivered treatment amendments within tight geological formations, demonstrating the actual achieved distribution using conventional borehole drilling methods can be both ineffective and cost prohibitive. Conceptual models of fracture and amendment distribution patterns are typically based on relatively small soil core and groundwater monitoring datasets, and therefore, are generally accompanied by high uncertainty. This uncertainty can lead to incorporation of large safety factors in full-scale remedial designs, as it is necessary to err on the conservative side when estimating parameters associated with remedial and delivery strategies (e.g., the number of injection wells, fractures, and spacing of those fractures needed to achieve remediation within a specific timeframe). With the ability to reduce design uncertainty, future remedial applications have the potential to be significantly more cost-effective.

This demonstration is based on the premise that geophysical imaging of emplacement of amendments via hydraulic fracturing can reduce the uncertainty in the design phase as well as the performance monitoring stage, thereby increasing efficacy and cost-effectiveness of the remedial treatment. The study focused on monitoring processes associated with Hydrogen Release Compound (HRC[®]), which is a slow release polylactate electron donor. HRC[®] and hydraulic fracturing were used for the remedial action (RA) at Spill Site 7 (SS7), located at F.E. Warren Air Force Base (FEW), to treat trichloroethene (TCE) and its degradation products in groundwater. The conceptual model of fracture installation used to develop the full-scale RA for SS7 is shown on Figure 2. This demonstration involved an *in situ* bioremediation pilot test at Plume E, a plume of TCE contaminated groundwater also at FEW, that was based upon the full-scale RA implementation at SS7. Additional information on site location, geology, hydrogeology, and contaminant distribution at FEW is provided in Section 4.

The results of this study are anticipated to be transferable to other bioremediation amendments (e.g., emulsified vegetable oils, other soluble carbon amendments, etc.) introduced using different strategies (e.g., pneumatic fracturing, traditional injection, jetting, etc.), provided that the geophysical attributes are sensitive to the injectates or their end products. Future applicability may also extend to other remedial approaches such as *in situ* chemical oxidation (ISCO) or *in*

situ chemical reduction. As such, the use of geophysical datasets to build a conceptual model of fracture imaging and amendment delivery may be applicable to other DoD sites where *in situ*

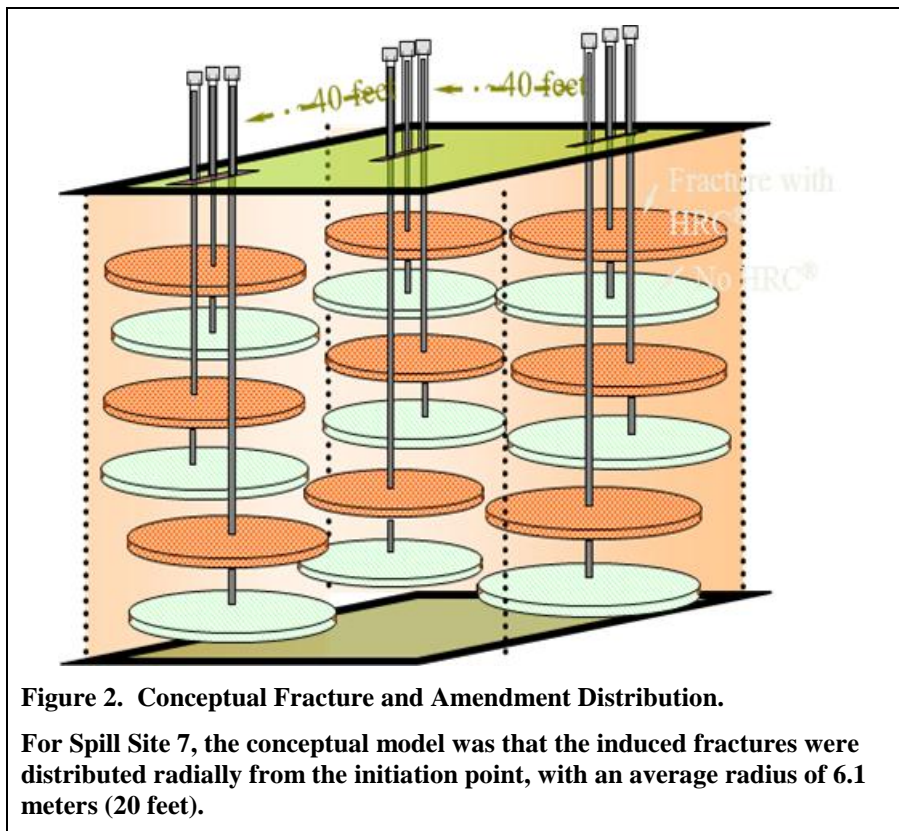


Figure 2. Conceptual Fracture and Amendment Distribution.

For Spill Site 7, the conceptual model was that the induced fractures were distributed radially from the initiation point, with an average radius of 6.1 meters (20 feet).

remediation is under consideration and/or applicable. An improved model is expected to lead to improved remediation efficacy and potentially lower cost associated with treatment materials and field implementation.

1.2 Objectives of the Demonstration

The objectives of this demonstration were to (1) assess the utility of time-lapse geophysical methods for monitoring fracture development and ability of fractures to distribute the remedial amendment, and (2) use that information together with conventional soil core and groundwater monitoring data to quantify the cost-benefit of using geophysical methods to develop an optimal delivery strategy prior to full-scale remedial action. Seismic, radar, and electrical geophysical methods were considered for this study.

1.3 Regulatory Drivers

There are no regulatory drivers specifically initiating the work included in this ESTCP project. However, FEW is a Comprehensive Environmental Response, Compensation, and Liability Act (CERCLA) site and the primary Remedial Action Objective (RAO) for SS7 and Plume E is to restore groundwater to drinking water standards (i.e., maximum contaminant levels [MCLs]) for TCE and its degradation products. The target contaminants and their applicable MCLs are:

- TCE (5 micrograms per liter [$\mu\text{g/L}$]);
- *cis*-1,2-dichloroethene (*cis*-1,2-DCE) (70 $\mu\text{g/L}$);
- *trans*-1,2,-dichloroethene (*trans*-1,2-DCE) (100 $\mu\text{g/L}$); and
- Vinyl chloride (2 $\mu\text{g/L}$).

Although the regulatory drivers listed above are specific to SS7 and Plume E, these cleanup levels are typical among other DoD facilities where groundwater remediation is considered and/or RAs are implemented.

The *in situ* bioremediation and monitored natural attenuation (MNA) RA at SS7 is considered “in place” and “Remedy In Place” status has been approved by the Wyoming Department of Environmental Quality (WDEQ) and United States Environmental Protection Agency (USEPA) Region 8. Restoration will be considered fully achieved when concentrations of the target contaminants in groundwater are reduced to their respective MCLs, as indicated above.

MNA was implemented at Plume E, which also is considered to have “Remedy In Place” status by WDEQ and USEPA Region 8. This study may support the existing MNA remedy at Plume E by potentially reducing contaminant concentrations within the higher concentration areas of the intermediate groundwater zone (e.g., between approximately 13.7 and 19.8 m [45 and 65 ft] below ground surface [bgs]).

SECTION 2 – TECHNOLOGY

This study included the testing of a novel, integrated approach using time-lapse seismic, radar, and electrical attributes to monitor and detect the distribution of amendments introduced via hydraulic fracturing at Plume E. In addition to responding to *in situ* heterogeneity, three classes of geophysical responses are expected to be associated with the remediation strategy, as follows:

- Responses related to the initial hydraulic fracturing. We hypothesized that fracture emplacement processes would primarily affect seismic signatures through the initial creation of fractures, pore pressure alteration, and rapid mechanical consolidation. Because seismic attributes (velocity and amplitude) are sensitive to elastic parameters and density, seismic methods were expected to be useful for monitoring fracture propagation and emplacement. In particular, we hypothesized that the induced fractures would lead to a decrease in primary wave (P-wave) velocity and an increase in attenuation. Due to the high resolution offered by crosshole radar and its sensitivity to changes in dielectric constant associated with the geology, we also considered radar as a fracture monitoring approach. We expect that these geophysical responses would occur almost immediately following fracture emplacement, with fracture growth occurring over minutes to hours, pore pressure dissipation occurring over similar time frames, and fracture healing occurring over a longer period dependent on the plastic behavior of the geological formation.
- Responses related to amendment distribution properties within fractures and diffusion into the formation. We hypothesized that electrical methods would be most effective at imaging initial amendment distribution within the fractures, due to its sensitivity to changes in pore fluid total dissolved solids (TDS). In particular, we hypothesized that the replacement of the fracture proppants with HRC[®] would slightly increase the electrical conductivity, and the replacement of the formation pore fluid with the amendment would significantly increase the effective electrical conductivity. Given the unique dielectric signature of HRC[®] (Hubbard et al. 2008), we also hypothesized that radar velocity could be used to monitor the amendment distribution.
- Responses related to biogeochemical transformations associated with the treatment, potentially including guar breakdown, the long-term utilization of carbon source, and associated carbon dioxide (CO₂) bubble generation and pH changes, which could dissolve caliche in the vicinity of the injection boreholes. Since these transformations lead to changes in the pore fluid concentration, we hypothesized that electrical methods would be the most effective remote monitoring approach; in particular, that the breakdown products would lead to an increase in bulk electrical conductivity.

In general, our conceptual model was that wave-based methods (seismic and radar) would be most effective at monitoring fracture emplacement and that electrical methods would be most effective at monitoring pore fluid geochemical changes. Due to the limitation in wellbore separation distances, and based on our preliminary field testing, radar signal propagation in the field was limited. As such, we primarily focused on understanding and testing the seismic and electrical responses to fracture emplacement and amendment distribution. This section includes technical background for these two approaches and provides a discussion of the advantages and limitations of the focus technology guiding the development of amendment delivery conceptual models.

2.1 Technology Description

This study explored the utility of seismic and electrical methods for monitoring the distribution of induced fractures and amendments, respectively. A common time-lapse strategy was used for all methods, and two different acquisition geometries were tested. The time-lapse strategy entails collecting data before and at several time steps after the treatment (in this case, after fracture and amendment emplacement) at the same location and subtracting the baseline dataset from the subsequent datasets. This procedure removes the effect of the geology on the geophysical signature and highlights changes to the signature caused by treatment or system response to treatment (Figure 3a). Crosshole seismic, electrical, and radar datasets were collected by inserting a geophysical source into one wellbore and recording the responses at another wellbore, and repeating this process over several different wellbore depths and wellbore pairs (Figure 3b). Surface electrical datasets were collected by placing electrodes along the ground surface (Figure 3c). These methods are briefly described below.

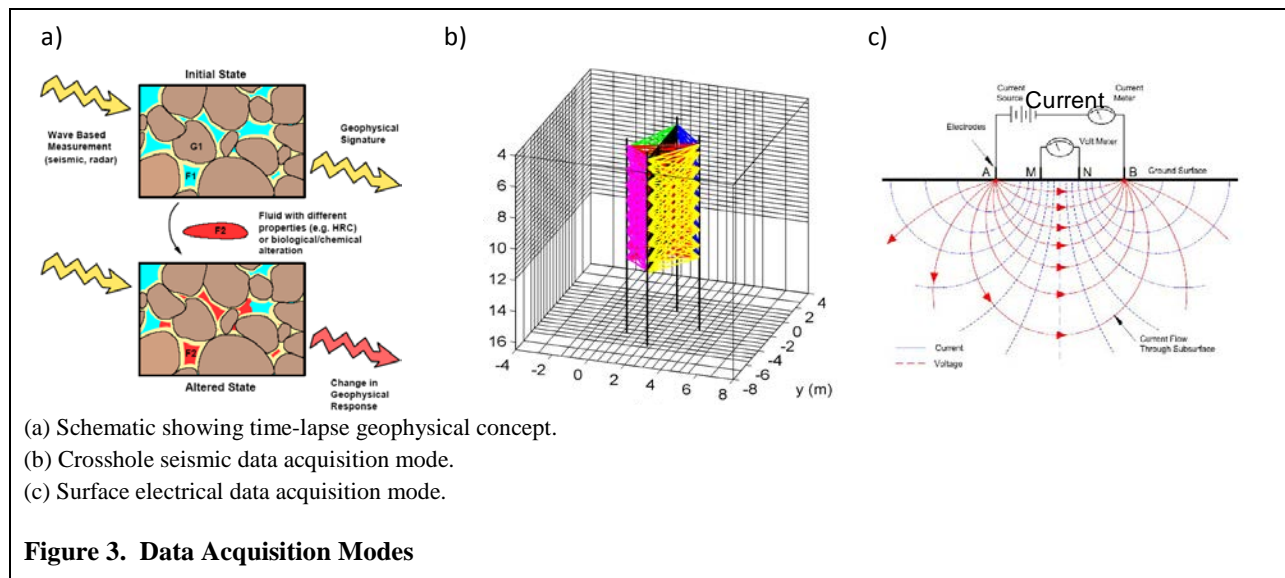


Figure 3. Data Acquisition Modes

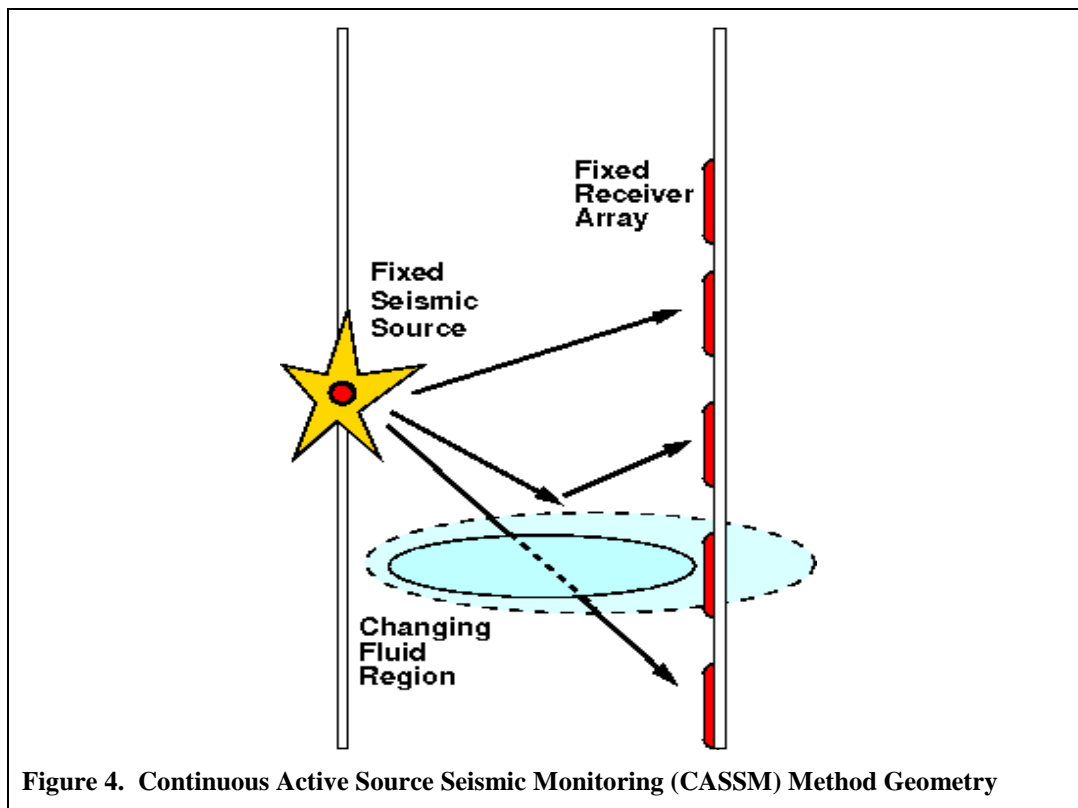
2.1.1 Seismic Methods

Seismic methods common to near subsurface investigations typically use high-frequency (approximately 100 to 5000 hertz [Hz]) pulses of acoustic energy to probe the subsurface. These pulses are generally artificially produced (using weight drop, hammers, explosives, piezoelectric transducers, etc.) and propagate outward as a series of wavefronts. The passage of the wavefront creates a motion that can be detected by a sensitive detector (geophone or hydrophone). According to the theory of elasticity upon which seismic wave propagation is based, several different waves are produced by a disturbance; these waves travel with different propagation velocities that are governed by the elastic constants and density of the material. The P-wave energy propagates as local compression and rarefaction of a unit volume, exhibiting longitudinal particle motion in the direction of the propagating wave. Transverse waves, also called secondary or shear (S)-waves, exhibit particle motions orthogonal to the propagation direction and have lower velocities than P-waves, and therefore, arrive later in the recording. P-wave arrivals are the easiest to detect and most commonly used arrival; we focus here on information

available from P-waves although a novel S-wave source was also tested during the project (see appendix E).

For the seismic method, two different crosshole approaches were explored, including: 1) a high frequency (“standard tomographic”) approach that provides excellent spatial coverage but limited temporal resolution, and 2) a high-frequency approach that provides excellent temporal resolution but limited spatial coverage (e.g., continuous active source seismic monitoring [CASSM]). CASSM instrument fabrication and testing by Lawrence Berkeley National Laboratory (LBNL) represented firsts for environmental remediation monitoring.

The standard tomographic imaging approach entails manually placing and moving a seismic source and a string of geophones over various depth intervals within wellbores to yield dense coverage of seismic waves in the inter-wellbore area. This method yields high spatial resolution. However, since repositioning of the seismic sensor strings is manual, the datasets tend to be collected only intermittently and often with sensor positioning errors, leading to low temporal resolution. In contrast with the standard tomographic approach, the CASSM system includes: 1) an array of 10 high-frequency piezoelectric sources, which are permanently positioned within a wellbore and autonomously and sequentially activated by a high-power amplifier; and 2) two independent receiver arrays (24 and 48 levels), which can be positioned in receiving wellbores. Figure 4 illustrates the CASSM method geometry.



The unique aspect of the CASSM approach is that it allows highly repeatable active source seismic imaging with a fine temporal resolution; this enables the technique to autonomously and accurately image fast processes which cannot be effectively monitored using the standard

tomographic seismic method. The fabricated geometry (10 sources times 72 receivers) was expected to provide sufficient data for travel time tomography along two planes that traversed the region expected to be impacted by fracturing. As each tomographic dataset can be acquired in a fully automatic mode in approximately 3 minutes, the CASSM monitoring data were expected to be able to image the fracture propagation process. Analysis of both the standard and CASSM seismic datasets includes several pre-processing steps (geometry assignment, filtering, and gain application), manual picking of the first energy arrival times, and tomographic inversion of the picked times to yield images of changes in P-wave velocity and attenuation (detailed in the following sections). Crosswell seismic imaging using an orbital shear wave source was viewed as an “opportunity” that was not identified in the original proposal; analysis of these data is still in progress and is not included in this report.

2.1.2 Electrical Resistivity Method

Electrical resistivity (the reciprocal of electrical conductivity) is an intrinsic property of a material representing its resistance to a current flow. In electrical resistivity methods, at low frequencies (<1 Hz), measured energy loss via ionic and electronic conduction dominates. Ionic conduction results from electrolytes filling interconnected pore space as well as from surface conduction via the formation of an electrical double layer at the grain-fluid interface (Revil and Glover 1997, 1998). The electrical current distribution can be visualized by equipotential surfaces, with current flow lines running perpendicular to these surfaces. Most resistivity surveys utilize a four-electrode measurement approach. The current is injected into the ground between two current electrodes, while one or more pairs of potential electrodes are used to measure electrical potential differences (or voltage). The measurement of this current and voltage, together with the geometric factor which is a function of the particular electrode configuration and spacing, is used to calculate resistivity for uniform subsurface conditions following Ohm’s law. Modern multi-channel geoelectrical equipment now includes multiplexing capabilities and automatic and autonomous computer acquisition, which greatly facilitate data acquisition within acceptable timeframes. Such surface imaging, now commonly called electrical resistivity tomography or ERT, allows the electrodes (tens to hundreds) to be used alternatively as both current and potential electrodes to obtain two- or three-dimensional (2D or 3D, respectively) electrical resistivity models. For our pilot study, ERT data were collected using electrode strings fabricated at LBNL and permanently installed in the subsurface. The electrode strings were placed along the ground surface as well as in boreholes, using both 2D and 3D geometries.

2.1.3 Geophysical Data Inversion, Interpretation, and Assessment

The geophysical measurements were inverted using previously developed codes to yield the following geophysical attributes: seismic velocity, seismic attenuation coefficient, radar velocity, radar attenuation coefficient, and electrical resistivity. Seismic data inversion was performed using both commercially available techniques and novel inversion techniques developed at LBNL (e.g., Ajo-Franklin 2007), which are specifically tailored for time-lapse analysis of injection processes. The resulting time-lapse image suites were then interpreted in terms of fracture and amendment distribution using site-specific petrophysical models that were developed based on laboratory studies conducted as part of this project (see Appendix A). As part of the assessment process, geophysical interpretations were compared to data collected from traditional measurements, such as groundwater and core measurements. Based on validated fracture and amendment distribution information obtained from the different geophysical

methods, several acquisition scenarios were developed for the cost-benefit analysis. This included assessing how much it would cost to collect a single geophysical monitoring dataset versus suites of geophysical datasets during a pilot study relative to the respective improvements in quantifying the region impacted by fracturing, and assessing how such information and costs translated into cost savings associated with a full-scale treatment.

2.2 Advantages and Limitations of the Technology

Physical fracture extent and general fracture characteristics are typically evaluated using conventional post-injection confirmation soil borings. The soil boring approach can be sufficient if the borings penetrate the impacted region and especially if the amendments are colored (e.g., purple potassium permanganate). For the SS7 RA, the location of fractures and the migration of byproducts associated with HRC[®] were difficult to assess in the field. Therefore, the fracture quantity and distribution, as well as the diffusion rates used to develop the conceptual model of HRC[®] distribution, were based upon observations of potassium permanganate diffusion observed at neighboring groundwater plumes where hydraulic fracturing with potassium permanganate was used as a groundwater remedy. Although such assumptions are not uncommon, they contribute to significant uncertainties in the delivery strategy conceptual model. In practice, these uncertainties often lead to higher than necessary implementation costs, as it is necessary to err on the conservative side when estimating parameters associated with the injection strategy, such as the number of injection wells or fracture zones, horizontal fracture initiation point spacing, and vertical spacing of fractures that are deemed necessary to remediate a given plume. *The greatest advantage of using geophysical technologies for designing an amendment delivery strategy is that they are minimally invasive and offer excellent spatial coverage relative to conventional soil boring methods, which together facilitate an improved understanding of in situ fracture and amendment distribution.* The guiding premise of this study is that the improved spatial resolution will lead to a fracture/amendment distribution model that has more certainty than soil boring- and groundwater monitoring-based models, which will in turn lead to lower overall remedial implementation costs.

There are several limitations to using geophysical datasets. The greatest limitation is that geophysical approaches provide indirect information only, such as changes in seismic velocity or electrical conductivity rather than presence of fractures or HRC[®] concentration; petrophysical models, either numerical or conceptual, are needed to interpret the geophysical responses to the treatment. A related limitation is that geophysical methods can be sensitive to more than one component of the experiment. For example, introduction of fractures, guar, and HRC[®] may all influence a geophysical attribute, and therefore, care must be taken to deconvolve the contributions. For these reasons, laboratory experiments were conducted as part of this study to gain insight into the relative contribution of different aspects of the manipulation on the geophysical signature and potential for obtaining a unique signature of fracture zonation and HRC[®] distribution using multiple geophysical attributes.

The acquisition geometry and measurement support scale poses some risk to successful fracture and amendment monitoring. A general limitation of geophysical methods is that their measurement support scale is larger than the scale at which the physical or biogeochemical changes occur. Therefore, the geophysical imaging provides only an effective, or averaged geophysical response to fracturing, amendment distribution, or subsequent transformations. Geophysical averaging occurs over the support scale of the measurement, which varies with

method and acquisition parameters and configuration. The time-lapse geophysical measurements were expected to be able to indicate the spatial distribution of the region impacted by fracturing and HRC[®] emplacement, but they were not expected to be able to image, for example, if the fracture thickness is 1/8 inch versus 1/4 inch. The wellbore geometry used to collect the geophysical data must be selected with an assumption of the induced fracture geometry. In this study, we assumed that the fractures would be distributed in a uniform disk pattern surrounding the fracture initiation point. Such assumptions can limit the utility of the geophysical data, especially if the fracture extends outside of the geophysical monitoring region.

Another limitation of using geophysical data for quantifying subsurface systems is that artifacts associated with the acquisition geometry and inversion process are often present in the final attribute image and it can be difficult to separate artifacts when interpreting subsurface heterogeneity. However, such artifacts are minimized when using time-lapse approaches (as was used in this study) because they are effectively “subtracted out” of the resulting difference image.

SECTION 3 – PERFORMANCE OBJECTIVES

The quantitative and qualitative performance objectives for this study are described in Table 1.

Table 1. Performance Objectives

Performance Objective	Data Requirements	Success Criteria	Results
Quantitative Performance Objectives			
1. Fracture characteristics are similar in nature to those installed at SS7.	Collection of soil borings post-hydraulic fracturing.	Radii between 5.2 and 7.0 m (17 and 23 ft) from the fracture initiation location for 2,000 pounds of sand delivered.	Achieved. Observed a radius between 7.0 and 7.6 m (23 and 25 ft).
2. Quantify utility of geophysical methods for delineating physical fracture and HRC [®] radius of distribution.	Pre- and post-fracturing geophysical datasets, laboratory analysis, inversion approaches, and confirmation soil core evaluation.	Ability to estimate mean and variance of fracture and HRC [®] radius as a function of heterogeneity using geophysical datasets.	Partially achieved. Different individual geophysical datasets were used to estimate the mean horizontal distribution of the fractures (between 7.0 and 9.1 m [23 and 30 ft]). Combinations of data can also be used to increase confidence in the interpretation. ERT data were used to estimate the vertical and mean radius (5.2 m [17 ft]) of injected amendment. We chose to use a “scenarios” approach of examining individual datasets as well as combinations of datasets rather than estimating a variance associated with a single measurement approach.
3. Assess value of different geophysical approaches for guiding development of amendment delivery strategy for quality of data collected.	Understanding of information gained from different geophysical approaches (individually and in combination) about HRC [®] and fracture distribution. Understanding of the risk/cost incurred in over-design (e.g., additional wells, material, and labor) and in under-design (e.g., failed treatment) of full-scale remediation treatment	Geophysical information suggests that: a) HRC [®] can be adequately distributed in subsurface using 20% fewer wellbore fracture installations, thereby saving cost of over-design (labor and materials). b) Conceptual model of wellbore and fracture spacing for HRC [®]	Achieved 20% reduction in number of fracture initiation points.

Table 1. Performance Objectives

Performance Objective	Data Requirements	Success Criteria	Results
	from project environmental engineers.	distribution is not adequate to ensure effective treatment (thereby saving costs/risk of remediation failure).	
4. Cost-Benefit Analysis	<p>Interpretation of qualitative and quantitative performance objectives using integrated geophysical, geochemical, and soil core sample analyses.</p> <p>Understanding of costs incurred using geophysical monitoring methods (acquisition, inversion, interpretation) to estimate HRC[®] and fracture distribution relative to costs incurred using conventional methods (e.g., groundwater sampling, core recovery) methods to estimate fracture and HRC[®] distribution.</p> <p>Assessment of costs associated with SS7 full-scale remedial action using a design strategy based on soil core and groundwater monitoring based methods.</p>	Total project cost savings of 20% or more for estimated full-scale remedial action implementation incorporating geophysical imaging in a field-scale pilot test to reduce design uncertainty, based on SS7 pilot test to full-scale cost relationship.	Achieved 20% cost savings for sites greater than 4 acres and treatment zones with an ROI of 7.0 m (23 ft).
Qualitative Performance Objectives			
1. Determine which geophysical method (or combination of methods) provides the best information about fracture delineation	Estimation of fracture distribution using (a) individual geophysical methods, and (b) combined methods compared with validation coring.	Identification of single or suite of geophysical measurements that provide estimate of fracture distribution.	Achieved. The CASSM and high-frequency seismic methods provided the best information about fracture distribution of the methods tested. The CASSM provided the most cost-effective single monitoring approach.
2. Determine which geophysical method (or combination of methods) provides the best information about HRC [®] distribution.	Estimation of HRC [®] distribution using (a) individual methods, and (b) combined methods compared with validation wellbore data.	Identification of single or suite of geophysical measurement approaches that provide estimate of HRC [®] distribution.	Achieved. Crosshole, 2D ERT provided the best information about amendment distribution.

Table 1. Performance Objectives

Performance Objective	Data Requirements	Success Criteria	Results
3. Determine which geophysical datasets are optimal for monitoring both fracture creation and HRC [®] distribution.	Estimation of HRC [®] and fracture distribution using (a) individual methods, and (b) combined methods compared with validation wellbore data.	Identification of single or suite of geophysical approaches that provide estimate of both HRC [®] and fracture distribution.	Achieved. CASSM with high-frequency seismic tomography and crosshole 2D ERT provided the best suite of methods for monitoring both fractures and amendment distribution of the methods tested.
4. Assess field-ruggedness, required user experience, and overall signal-to-noise ratio of commercially available geophysical approaches for monitoring HRC [®] and fracture distribution.	Qualitative analysis of signal-to-noise ratio of electrical, high-frequency, and radar methods. Input from geophysicists and feedback from field technicians.	Information from at least one of the imaging systems is sufficiently robust for detecting HRC [®] and/or fractures and is interpretable by a skilled technician.	Achieved. Time-lapse ERT acquisition and inversion approaches are commercially available and could be used by a skilled technician to estimate amendment distribution.

Notes:

2D = two-dimensional

CASSM = continuous active source seismic monitoring

ERT = electrical resistivity tomography

ft = feet

HRC[®] = Hydrogen Release Compound[®]

m = meter

ROI = radius of influence

SS7 = Spill Site 7

SECTION 4 – SITE DESCRIPTION

FEW is located west of the city of Cheyenne, in south-central Laramie County in southeastern Wyoming (Figure 5). From a contaminant perspective, FEW is divided into three zones: Zone D, Zone B, and Zone C. Zone D is generally defined as the portion of FEW bounded by Roundtop Road along the western boundary of the base (Figure 6), Crow Creek to the north and east, Diamond Creek to the northwest, Zone B to the southwest, Zone C to the southeast, and Happy Jack Road along the southern boundary of the base. Zone D contains five groundwater plumes contaminated with TCE and its degradation products (e.g., *cis*-1,2-DCE, *trans*-1,2-DCE, and vinyl chloride) at concentrations exceeding federal MCLs (USAF 2006a).

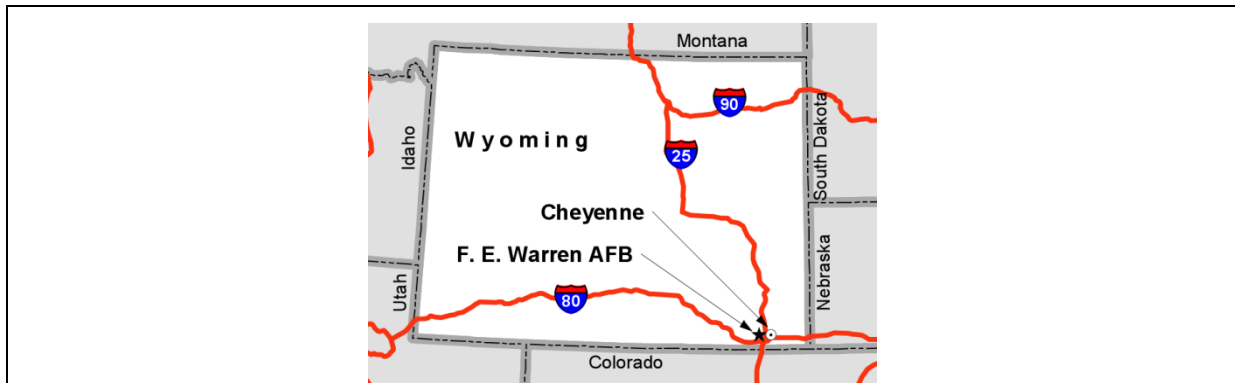


Figure 5. F.E. Warren Air Force Base Site Location

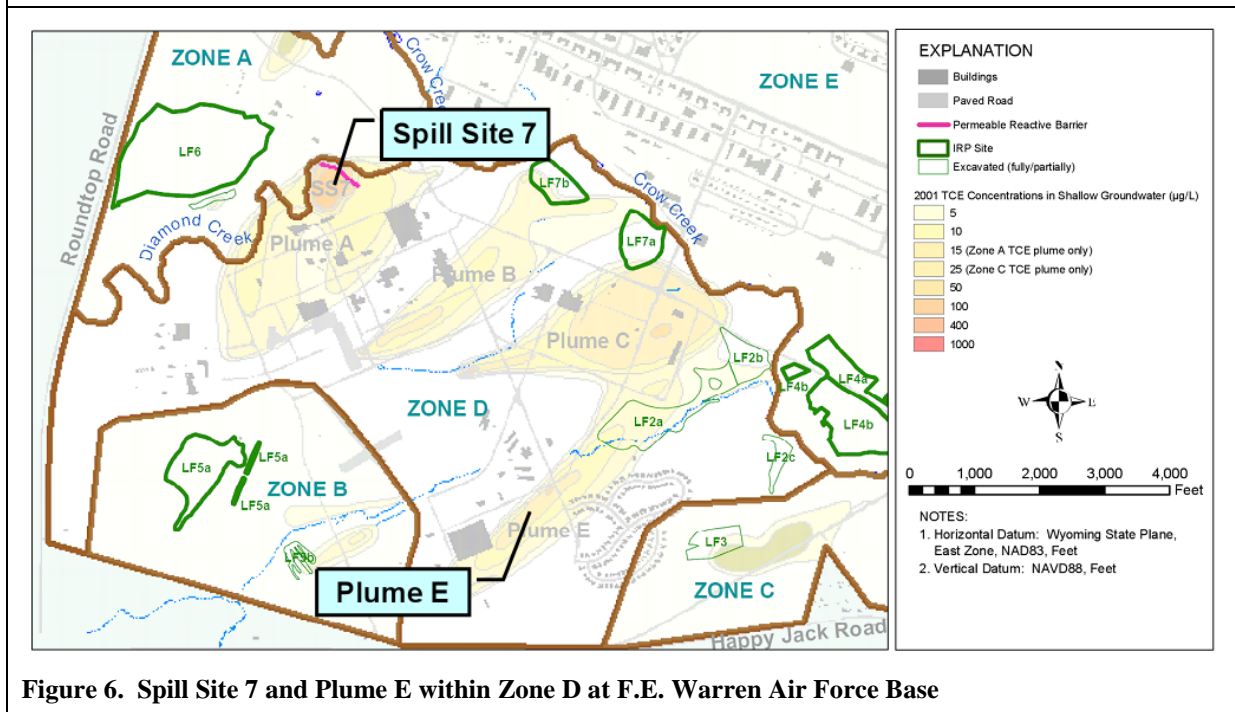


Figure 6. Spill Site 7 and Plume E within Zone D at F.E. Warren Air Force Base

FEW was selected for this project based on three primary factors: 1) the understanding of site geology, 2) previous experience with hydraulic fracturing, and 3) quantified cost of a full-scale RA using a hydraulic fracturing and HRC[®] approach.

Geology at FEW is highly heterogeneous with low permeability aquifer materials throughout the installation. Although variability exists across the installation, previous investigative, remedial design, and remedial implementation work performed across FEW allows for a comprehensive understanding of general site lithology and extent of contaminant plumes. Because of the low-permeability lithology at FEW, non-traditional amendment delivery methods have been used to implement selected groundwater remedial alternatives.

The quantity and quality of site geology and hydraulic fracturing data compiled for FEW made it a sound location choice for implementing this demonstration. One of the five TCE groundwater plumes, Plume E, was selected for this demonstration because of its lithology, available monitoring network, depth range of contaminant and lithologic data, contaminant concentrations, and lack of previous intrusive remedial activities. Primarily, intrusive pilot testing and/or hydraulic fracturing have not been implemented at Plume E; therefore, the lithology is relatively undisturbed. The lithology observed at Plume E is heterogeneous and generally representative of the lithology across FEW.

4.1 Site Location

As shown on Figure 5, TCE Plume E is located to the south of Plume C, next to the southeast boundary of Zone D. A residential area, Carlin Heights, is located on a slight hill to the southeast of Plume E. The plume originates in the vicinity of Building 945, which is located at Mule Deer and Booker Roads, and extends approximately 1,525 m (5,000 ft) downgradient (northeast) to Crow Creek. The demonstration was performed near the head of Plume E where TCE concentrations are generally the highest.

4.2 Site Hydrogeology

In general, the shallow stratigraphy at FEW consists of discontinuous lenses of fine grained sand and silt. The upper 6.1 to 7.6 m (20 to 25 ft) of the shallow saturated aquifer is made up of unconsolidated terrace and alluvial deposits. Below the alluvial deposits lies the Ogallala Formation, a mixture of clay, silt, poorly sorted sand, and gravel layers. Some of the sand and gravel layers have been cemented to create discontinuous sandstone and conglomerate beds. The terrace and alluvial deposits and the upper Ogallala Formation combine to form an unconfined aquifer at the installation.

The transitions between strata in the unconfined aquifer are often subtle, with one layer grading into the next. This makes it difficult to correlate distinct hydrostratigraphic units. For this reason, a simpler method of identifying hydrostratigraphic units was developed during previous investigations and RAs at FEW, which involves dividing the shallow aquifer into separate layers according to depth below the groundwater table. Three layers were defined starting at the top of the groundwater table: Layer 1 (shallow) spans the upper 6.1 m (20 ft) of the saturated zone; Layer 2 (intermediate) extends 9.1 m (30 ft) below the bottom of Layer 1; and Layer 3 extends 12.2 m (40 ft) below the bottom of Layer 2. These layers provide the basis for the shallow, intermediate, and deep aquifer zones that are referenced in subsequent FEW reports and figures. The combined aquifer thickness is assumed to be approximately 27.4 m (90 ft).

Throughout most of the site, groundwater levels are approximately 3.0 to 6.1 m (10 to 20 ft) bgs. In the floodplain of Crow Creek and the vicinity of a small tributary (the Unnamed Tributary) that crosses a downgradient portion of the plume, depths to groundwater decrease to less than

1.5 m (5 ft). Groundwater levels are generally stable, with seasonal variations from a couple of feet up to 5 feet. These fluctuations are due to groundwater recharge from precipitation and snowmelt. The overall stability of the groundwater potentiometric surface suggests that it represents the steady-state (i.e., long-term average) condition of the groundwater flow system.

During the Zone D Remedial Investigation (RI) (USAF 2003), the horizontal hydraulic gradient for areas away from Crow Creek was calculated at 0.003 m/m (0.01 ft/ft). As groundwater flow approaches the creek, hydraulic gradients perpendicular to the creek increase to 0.018 m/m (0.06 ft/ft). This appears to be the result of the relatively low permeability of terrace deposits that flank the creek. In the Crow Creek floodplain, groundwater flow was found to change direction by almost 90 degrees to flow parallel to the creek, at a reduced gradient of approximately 0.001 m/m (0.004 ft/ft).

Vertical hydraulic gradients are apparent at several well clusters in Zone D. Most of the well clusters indicate a downward gradient, which suggests that groundwater recharge is occurring in these areas. Strong downward hydraulic gradients are present in the up-gradient reaches of Plume E. The vertical head difference is pronounced near the head of Plume E, where head differences up to 3.7 m (12 ft) have been observed in the DRMO-003 well cluster (shallow to intermediate). The downward gradient at the DRMO-003 well cluster may be indicative of vertical anisotropy.

The unconfined aquifer at FEW is heterogeneous with respect to hydraulic conductivity. Slug and pumping tests historically conducted at the installation have shown that hydraulic conductivity varies by as much as six orders of magnitude. Generally, horizontal conductivity values are highest in the shallow aquifer zone and lowest in the deep aquifer zone, a variation that is consistent with the aquifer geology. The unconfined aquifer is also anisotropic, and exhibits higher hydraulic conductivity in the principal groundwater flow direction, which is to the northeast throughout most of Zone D. Vertical hydraulic head differences observed across the study area suggest that the vertical hydraulic conductivity is smaller than the horizontal hydraulic conductivity. This is likely due to the physical layering and compaction process of alluvial deposition.

Plume E includes several well locations with relatively coarse-grained sediments in the intermediate zone aquifer. For example, the lithology at the DRMO-003 well cluster is predominantly clay and fine-grained sediments in the shallow aquifer zone, but transitions to sand and silty sand in the intermediate aquifer zone. The variation in hydraulic conductivity between the shallow clayey sediments and the intermediate sandy sediments may explain the 12 foot downward vertical gradient observed at this well cluster. Other Plume E wells contain coarser-grained sediments in the intermediate aquifer zone. These intervals of coarse-grained sediments suggest that hydraulic conductivity could be higher in the Plume E intermediate aquifer than the rest of the intermediate aquifer zone at Zone D.

Slug test data also suggest that the Plume E intermediate aquifer zone has a relatively high hydraulic conductivity. Base-wide, the geometric mean for intermediate aquifer zone slug tests was 0.09 m/day (0.30 ft/day). By comparison, two slug tests conducted at the Plume E intermediate aquifer zone had estimated hydraulic conductivity values of 1.2 and 5.5 m/day (4 and 18 ft/day) (USAF 2003).

4.3 Contaminant Distribution

Plume E was selected as the site for the dynamic field test following an assessment of its geological and chemistry data and preliminary geophysical testing described in the Demonstration Plan (LBNL 2010). Plume E originates in the vicinity of Building 945 (Figure 7), a former motor pool maintenance facility, and extends approximately 1,525 m (5,000 ft) downgradient toward Crow Creek. The operational history of Plume E is not well known and a discrete source area was not identified for the plume during the Zone D Source Areas RI (USAF 2006b).

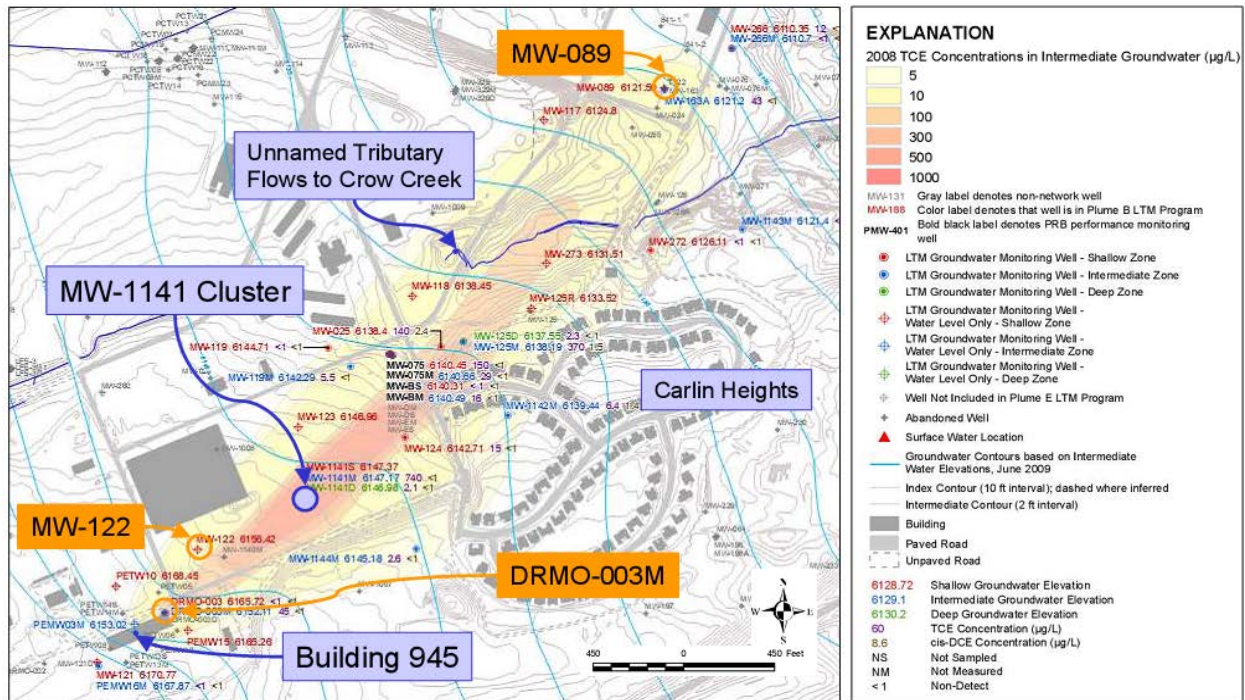
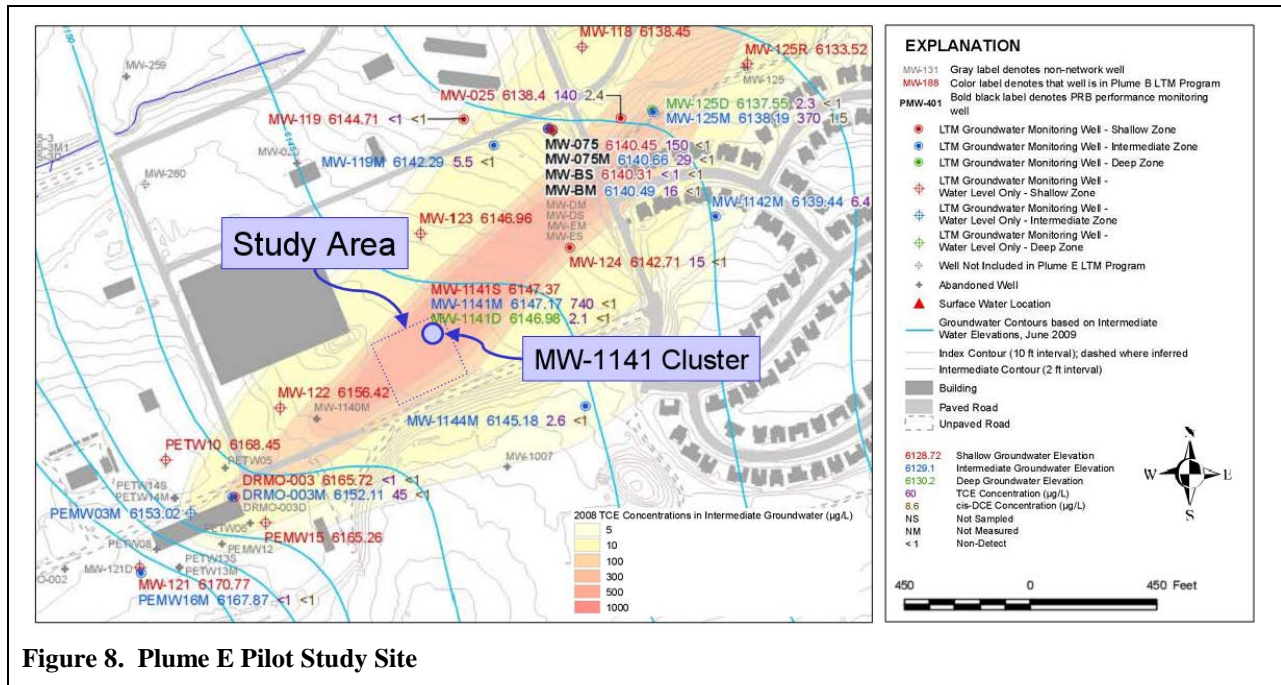


Figure 7. Plume E Intermediate Groundwater Trichloroethene Concentration Contours

This site was selected primarily because 1) the upper portion of Plume E does not include implemented active remedies (i.e., MNA only) and has measurable TCE concentrations, and 2) Plume E has data for a large vertical depth range of saturated material spanning the shallow, intermediate, and deep aquifer zones, allowing multiple fracture depths and study of lithological effects.

The pilot study site is situated near monitoring well cluster MW-1141, which is located within the study area (Figure 8) and is representative of contaminant concentrations in that area. The screened intervals and example TCE concentrations for the MW-1141 well cluster are summarized below:



- The shallow aquifer zone is screened from approximately 7.3 to 10.4 m (24 to 34ft) bgs with a TCE concentration of approximately 45 µg/L, as detected in September 2007;
- The intermediate aquifer zone is screened from approximately 15.1 to 18.1 m (49.5 ft) bgs with a TCE concentration of approximately 848 µg/L, as detected in June 2008; and
- The deep aquifer zone is screened from approximately 25 to 28 m (82 to 92 ft) bgs with a TCE concentration of approximately 4.5 µg/L, as detected in June 2008.

TCE breakdown products (e.g., *cis*-1,2-DCE, *trans*-1,2-DCE, and vinyl chloride) have not been detected within any of the aquifer zones at the MW-1141 well cluster.

SECTION 5 – TEST DESIGN

This section provides a detailed description of the study design and testing performed to address the quantitative and qualitative performance objectives described in Section 3. Specific activities conducted in preparation of and during the Spring 2010 dynamic pilot test are included in this section.

5.1 Conceptual Experimental Design

This demonstration involved an *in situ* bioremediation pilot test at Plume E that was based upon the full-scale RA implementation at SS7. The pilot test involved multiple tasks, including: collecting and evaluating data, comparing data to the 2006 full-scale RA implementation at SS7, and performing a cost-benefit analysis.

The pilot test was performed in an untreated region of Plume E. HRC[®] was delivered to the subsurface via hydraulic fracturing using practices similar to those used at SS7. Fracture emplacement and delivery of HRC[®] was monitored using time-lapse geophysical methods as well as more conventional soil boring approaches.

The pilot test included the following key tasks:

1. Installation of geophysical wellbores;
2. Collection of baseline geophysical and groundwater samples for laboratory analysis;
3. Installation of one hydraulic fracture within the shallow aquifer zone (i.e., Layer 1) at approximately 11.6 m (38 ft) bgs;
4. Installation of one hydraulic fracture with HRC[®] within the intermediate aquifer zone (i.e., Layer 2) at approximately 14.3 m (47 ft) bgs; and
5. Collection of post-fracturing time-lapse geophysical datasets and conventional monitoring data, including soil borings for laboratory analysis.

The pilot test enabled the exploration of field-scale geophysical responses to both fracture creation and HRC[®] distribution in the presence of natural heterogeneity, and therefore, permitted an assessment of the value of the technology for aiding in development of an optimal delivery strategy. Geophysically-inferred features and properties were then confirmed using secondary soil borings and core analyses in order to evaluate the performance objectives presented in Section 3 (Table 1). Further details of this dynamic pilot test are provided below.

5.2 Baseline Field Characterization Activities

To assist with field plan design and interpretation of geophysical data in terms of fracture and amendment distribution, we performed several laboratory studies that involved components and mixtures of components collected from the subsurface at Plume E, including: guar, HRC[®], groundwater, and sediments. An environmental geophysics laboratory at LBNL was used to co-collect geochemical, hydrological, and geophysical datasets (Figure 9). Experiments were carried out at the Environmental and Applied Geophysics Laboratory (EAGL) at LBNL and included geochemical, hydrological, and geophysical datasets. Details of the laboratory experiments are described in the Demonstration Plan (LBNL 2010) and summarized in Appendix A.



Figure 9. Laboratory Setup and Team Members Jonathan Ajo-Franklin and Yuxin Wu

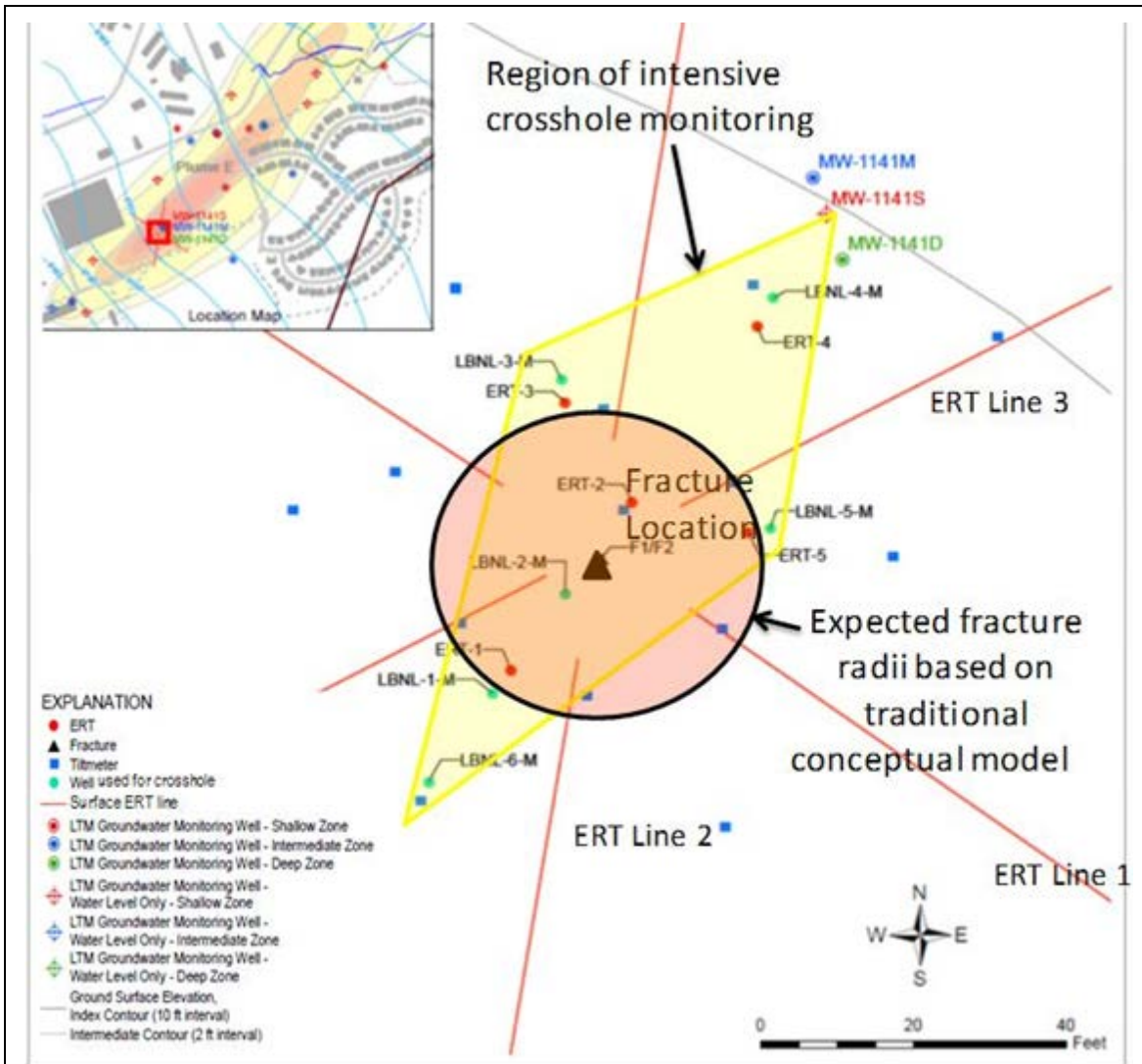
5.2.1 Plume E Field Investigation

To provide general subsurface geology and plume location, and aid the selection of fracture locations, surface ERT surveys were conducted using an AGI SuperSting R8/IP system to select the specific location for the pilot study. Details regarding the 2009 surface ERT survey are included in the Demonstration Plan (LBNL, 2010). Results from the surface ERT data are consistent with preexisting geochemical and lithological information and were used to help select the location of the dynamic pilot study.

5.2.2 Pilot Study Site Selection, Development, and Baseline Geophysical and Groundwater Characterization

Geophysical boreholes were installed at Plume E in October 2009 in preparation for dynamic testing planned for Spring 2010. The intentions of increasing the time between the installation of test wells and the 2010 pilot study were to 1) allow maximum equilibrium of test wells with the native formation, 2) decrease the likelihood of surfacing via newly installed test wells, and 3) collect baseline geophysical datasets and groundwater parameters from the test wells that can be used to refine the pilot study experimental parameters, as needed.

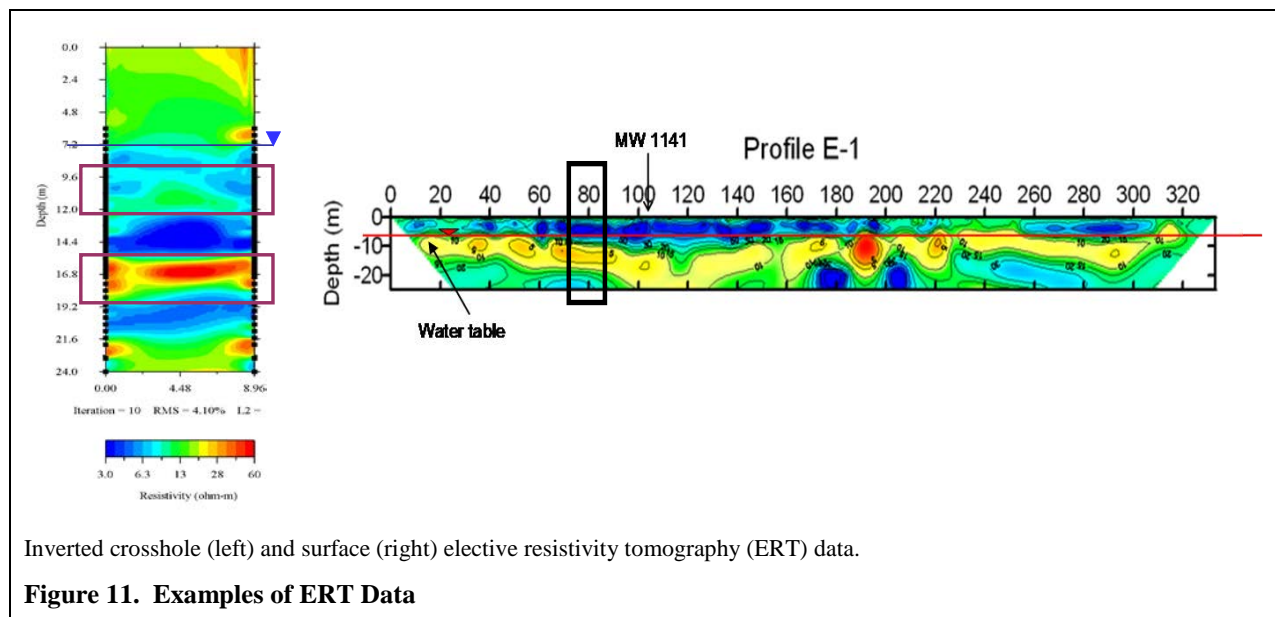
Eleven boreholes were advanced and completed as part of baseline activities including: five ERT boreholes, five seismic boreholes with 2-inch diameter well casings, and one orbital seismic borehole with a 4-inch diameter well casing (Figure 10). Well survey coordinates are provided in Appendix B. Soil cores for lithologic evaluation were collected at three boreholes during the 2011 confirmation soil boring sampling event. Results are discussed further in Section 5.4. Baseline groundwater monitoring within the intermediate aquifer zone was conducted at six locations.



Radius of influence estimated from SS7 (pink circle)
 Surface electrical resistivity tomography (ERT) lines (red lines)
 Crosshole imaging region (yellow diamond)
 ft = feet
 LTM = long-term monitoring

Figure 10. Pilot Study Layout.

Baseline geophysical characterization, including surface and crosshole acquisition, was conducted in May 2010 to gain an understanding about the site gross hydrogeological heterogeneity and to aid in selection of the fracture location intervals. Figure 11 shows an example of surface and crosshole ERT data collected during the pilot study, as well as the two chosen intervals for introducing fractures.



Baseline groundwater field parameters and samples were collected during the week of May 24, 2010. Monitoring locations included the MW-1141 well cluster as well as the four seismic wells. Groundwater parameters and laboratory analyses are included in Table 2.

Table 2. Pilot Test Performance Groundwater Parameters and Laboratory Analyses

Analysis ¹	Analytical Method	Field Instrument or Laboratory Analysis	Data Use
Water-level (groundwater)	Electric tape/flume	Field	Flow direction/elevation
pH	EPA SW-846 9040B	Field	pH values between 6 and 8 are optimal for microbial degradation
Water temperature	EPA 170.1	Field	Microbial metabolic rates are temperature dependent
ORP	Down-well instrument	Field	Less than -100 millivolts indicates strong anaerobic conditions have been established
Dissolved oxygen	Flow-through cell	Field	Concentrations <1 mg/L indicate anaerobic processes
Specific conductance	EPA SW-846 9050A	Field	General water quality parameter
Turbidity (groundwater)	EPA 180.1	Field	General water quality parameter
TCE	EPA SW-846 8260B	Laboratory	Existing target contaminant; Performance monitoring
Total 1,2-DCE	EPA SW-846 8260B	Laboratory	Not previously detected; indicates partial degradation
<i>trans</i> -1,2-DCE	EPA SW-846 8260B	Laboratory	Not previously detected; indicates partial degradation
<i>cis</i> -1,2-DCE	EPA SW-846 8260B	Laboratory	Not previously detected; indicates partial degradation
Vinyl Chloride	EPA SW-846 8260B	Laboratory	Not previously detected; indicates partial degradation
Anions ³	EPA SW-9056	Laboratory	Performance monitoring

Table 2 Notes:

¹ To optimize conditions for additional biostimulation and, if necessary, bioaugmentation, additional samples may be collected for total organic carbon (TOC), total and dissolved iron, ammonia, ortho-phosphate, volatile fatty acids (VFAs), sulfide and methane on an as needed basis based on monitoring data collected from previous sampling events.

² Including ethene and methane.

³ Anions may include analyses for nitrate, phosphate, and sulfate.

mg/L = milligrams per liter

cis-1,2-DCE = cis-1,2-dichloroethen

COC = constituent of concern

DCE = dichloroethene

EPA = U.S. Environmental Protection Agency

NA = not applicable

ORP = oxidation reduction potential

TCE = trichloroethene

trans-1,2-DCE = trans-1,2-dichloroethen

5.3 Pilot Study

Implementation of the *in situ* bioremediation pilot study at Plume E involved several field activities, which have been grouped into four phases and are discussed below.

5.3.1 Phase 1 – Site Preparation Activities

Site preparation activities included: 1) identifying and securing existing site features, such as monitoring wells, that were potential surface conduits for fracturing materials; 2) conducting baseline groundwater monitoring to verify current (i.e., pre-fracturing) site conditions (see Table 2); and 3) mobilizing personnel, materials, and equipment to the test site.

5.3.2 Phase 2 – Fracturing and HRC[®] Emplacement Activities

Field activities conducted for hydraulic fracturing and HRC[®] emplacement are described below.

5.3.2.1 Fracture Initiation Borehole Drilling

To create each fracture initiation location, a borehole was advanced from ground surface using solid stem augers attached to a dual capability direct push drill rig. The augers were advanced to at least 0.61 m (2 ft) above the shallowest targeted fracture depth, and then removed from the borehole. Using direct push drilling methods, 2-inch diameter temporary fracture casing (e.g., direct push rod approximately 2-inches outer diameter) was driven the remaining vertical distance to reach the first target fracture depth, creating the seal necessary for horizontal fracture initiation. When the target fracturing depth was reached, the casing was retracted to expose a 2-inch vertical section of open borehole. The fracture location was then notched to prepare the borehole for fracture initiation and propagation, further described in Section 5.3.2.2 below (Injection Well Installation and Completion). After the propagation of each fracture, direct push drilling resumed until the next target fracture depth was reached.

5.3.2.2 Fracture Propagation

To initiate fractures, a down-hole notching tool was inserted into the fracture initiation borehole. Notching was used to prepare the borehole for fracturing by creating a horizontal void space in the formation at the target fracture depth. This void space promotes fracture propagation in a horizontal direction during fracture initiation. The notching process is performed using a high-

pressure (e.g., approximately 3,500 pounds per square inch gage [psig]) water jet, and produces minimal quantities of both water and soil wastes.

The pressure at the notched area is increased until the formation “breaks” or allows initiation of the fracture; this effect was observed to occur at approximately 150 to 300 psig during previous fracturing work in other areas at FEW. Fractures were hydraulically installed into the shallow aquifer zone (approximately 11.5 m [38 ft] bgs) and the intermediate aquifer zone (approximately 14.3 m [47 ft] bgs). For each location, we attempted to deliver 2000 pounds of sand in a linked guar carrier with approximately 200 pounds of dyed HRC[®]. Sand, guar, and HRC[®] injection mass were manually recorded during emplacement to provide additional timing information for observed phenomenon. Photographs of the various aspects of the pilot study implementation are shown in Figure 12.

5.3.2.3 Injection Well Installation and Completion

Fracture initiation boreholes were completed as injection wells for the possible subsequent injection of microbial culture for bioaugmentation. Based upon previous work performed at FEW, the 1¾-inch injection wells were installed with one 1.5-m (5-ft) screen to access the emplaced fractures (e.g., one 1.5-m [5-ft] screen per fracture).

5.3.3 Phase 3 – Performance Monitoring Activities

Performance monitoring was conducted to evaluate aquifer redox conditions following fracturing activities, as described in the subsections below.

5.3.3.1 Groundwater Monitoring

Three months after electron donor emplacement, groundwater samples were collected from the performance monitoring well locations summarized in Table 3. The purpose of the performance groundwater monitoring was to evaluate initial reductions in contaminant levels. Due to the site geology, the intermediate aquifer zone fracture did not propagate at the target depth. As a result, the groundwater well screen interval (installed prior to the pilot study) was 0.9 m (3 ft) below the fracture zone. The field parameter and analytical data collected in July 2010 confirmed that the physical separation distance between the fractured zone and the well screen interval was too large to correlate, and therefore, data were inconclusive. For this reason, subsequent groundwater performance monitoring samples were not collected.

5.3.3.2 Post-Fracture Geophysical Monitoring

Post-fracturing geophysical response datasets were collected and processed during four events following the pilot study.

Table 4 shows the different types of data that were collected over time in association with the pilot study. In general, the standard seismic tomographic data and all of the crosshole and surface ERT were acquired along 10 cross-sections at specific time intervals over a 6-month period before, during, and after fracturing and injection of the HRC[®]. Over 1,000 CASSM crosshole datasets with a time-resolution of approximately 3 minutes were acquired between three wells over a 9 day period; the CASSM dataset spanned a baseline period, the fracturing events, and several days after the last fracture to allow monitoring of any fast consolidation processes which might be present.



Table 3. Groundwater Sample Collection Summary

Sample ID	Analyte(s) and Laboratory Method				
	VOCs (SW8260B)	Dissolved Metals (SW6010B)	Alkalinity (A2320)	Anions (SW9056A)	TOC/TIC (SW9060)
Baseline Groundwater Sampling – December 2009					
LBNL-2-M	X	X	X	X	X
LBNL-3-M	X				
LBNL-4-M	X				
LBNL-6-M	X	X	X	X	X
MW-1141D	X				
MW-1141M	X	X	X	X	X
MS-1141S	X	X	X	X	X
Performance Groundwater Monitoring – July 2010					
LBNL-2-M	X	X	X	X	X/X
LBNL-4-M	X	X	X	X	X/X
LBNL-5-M	X	X	X	X	X/X

TOC/TIC = total organic carbon/total inorganic carbon

Table 4. Geophysical Acquisition Times

Date	CASSM	Crosshole Seismic	Crosshole ERT	Crosshole 3D ERT	Surface ERT
May 24-28, 2010 (Baseline [Pre-Fracturing])	Begin May 28, 2010	All well pairs collected	All well pairs collected	Both 3D configurations collected	All three lines collected
June 1-3, 2010 (During Fracturing)	End June 5, 2010		Some well pairs collected	Both 3D configurations collected	All three lines collected
June 4-6, 2010 (Post-Fracturing)		All well pairs collected	All well pairs collected	Both 3D configurations collected	All three lines collected
June 8-10, 2010		All well pairs collected	All well pairs collected	Both 3D configurations collected	All three lines collected
August 26-28, 2010		All well pairs collected	All well pairs collected	Both 3D configurations collected	All three lines collected
October 13-15, 2010		All well pairs collected	All well pairs collected		All three lines collected

3D = three-dimensional CASSM = continuous active source seismic monitoring ERT = electrical resistivity tomography

In addition to geophysical monitoring, three supporting datasets were acquired during the pilot study: (1) a ground deformation network was established and surface displacement was measured using uplift stakes and a total station, (2) a network of tilt sensors was co-located with the 13 displacement stakes, and (3) injection pressure and flow rate were measured to provide basic constraints on fracture initiation and propagation as well as pressure diffusion after shut-in. Pressure gauges at the fracture well head and the pump were installed and recorded automatically during emplacement of both fractures. Results of the geophysical monitoring are discussed further in Section 5.4.2.

5.3.4 Phase 4 – Demobilization Activities

Demobilization field activities conducted after hydraulic fracturing and *in situ* bioremediation activities included borehole abandonment and surveying. Survey data are included in Appendix B.

5.4 Interpretation and Validation

Groundwater data, geophysical data, and validation wells were used to interpret the extent of both the fractures and amendment.

5.4.1 Groundwater Monitoring

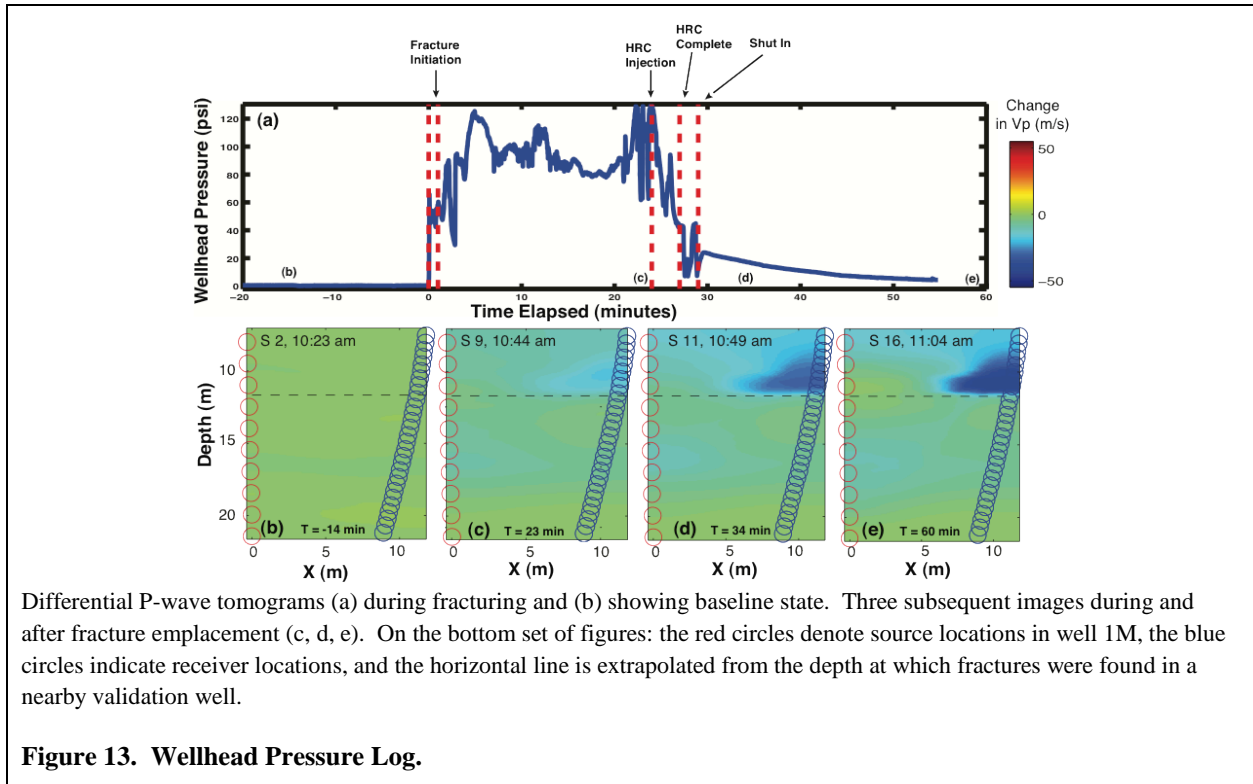
One round of post-fracturing performance monitoring was conducted in July 2010. Three locations were sampled and analyzed for the analytes listed in Table 3. As discussed in Section 5.3.3.1, due to an inability to install the intermediate aquifer zone fracture at the target depth, the intermediate well screens were installed 0.9 m (3 ft) below the fracture zone, and the vertical separation between the fracture zone and the well screens was too large to correlate the data with potential contaminant reductions relating to the treatment. Although well LBNL-2-M did show some reduction in TCE between baseline (980 µg/L) and the July 2010 post-emplacement performance monitoring (630 µg/L), in general the results were inconclusive with respect to potential contaminant reduction from the amendment emplacement. Results for wells LBNL-4-M showed a slightly increasing TCE concentration and LBNL-5-M did not have a corresponding baseline. Results from the baseline (December 2009) and post-fracturing (July 2010) groundwater monitoring events are included in Appendix C.

5.4.2 Geophysical Monitoring

All geophysical data collected after the fracture initiation began were differenced from the baseline datasets to obtain changes in seismic velocity, seismic attenuation, radar velocity, and electrical conductivity. Due to the wellbore separation distances and electrical conductivity of the subsurface, the radar signal was attenuated, and therefore, the signal-to-noise ratio was not high enough to interpret. Only the seismic and electrical monitoring datasets and their joint interpretation are described herein.

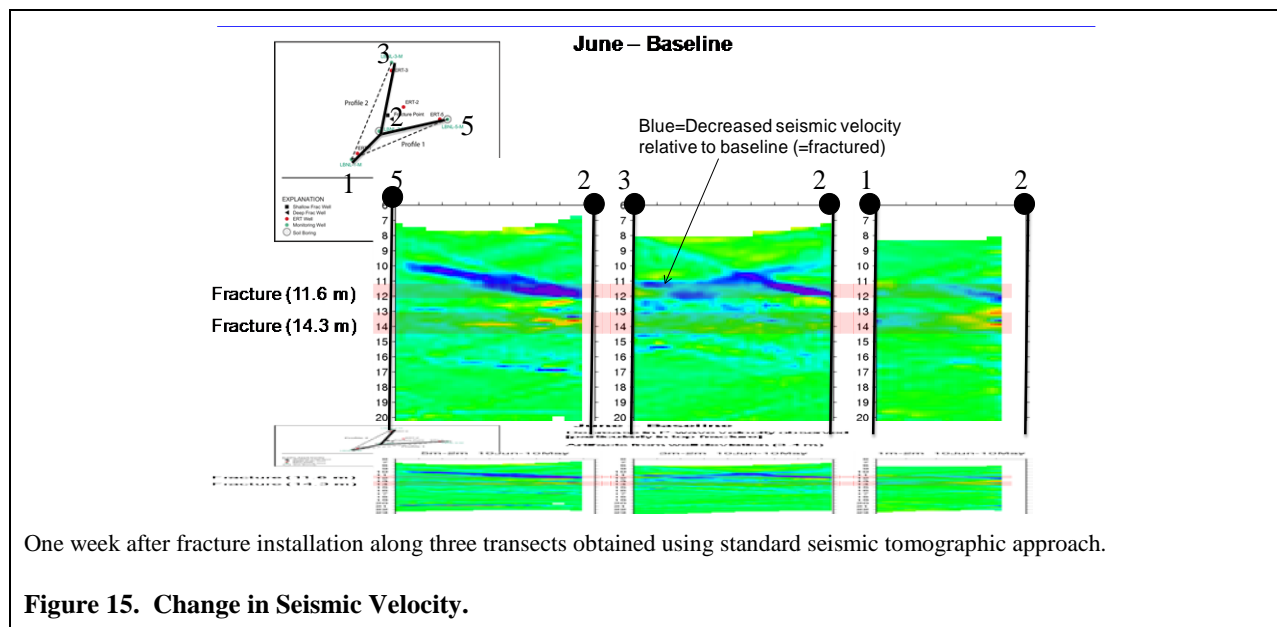
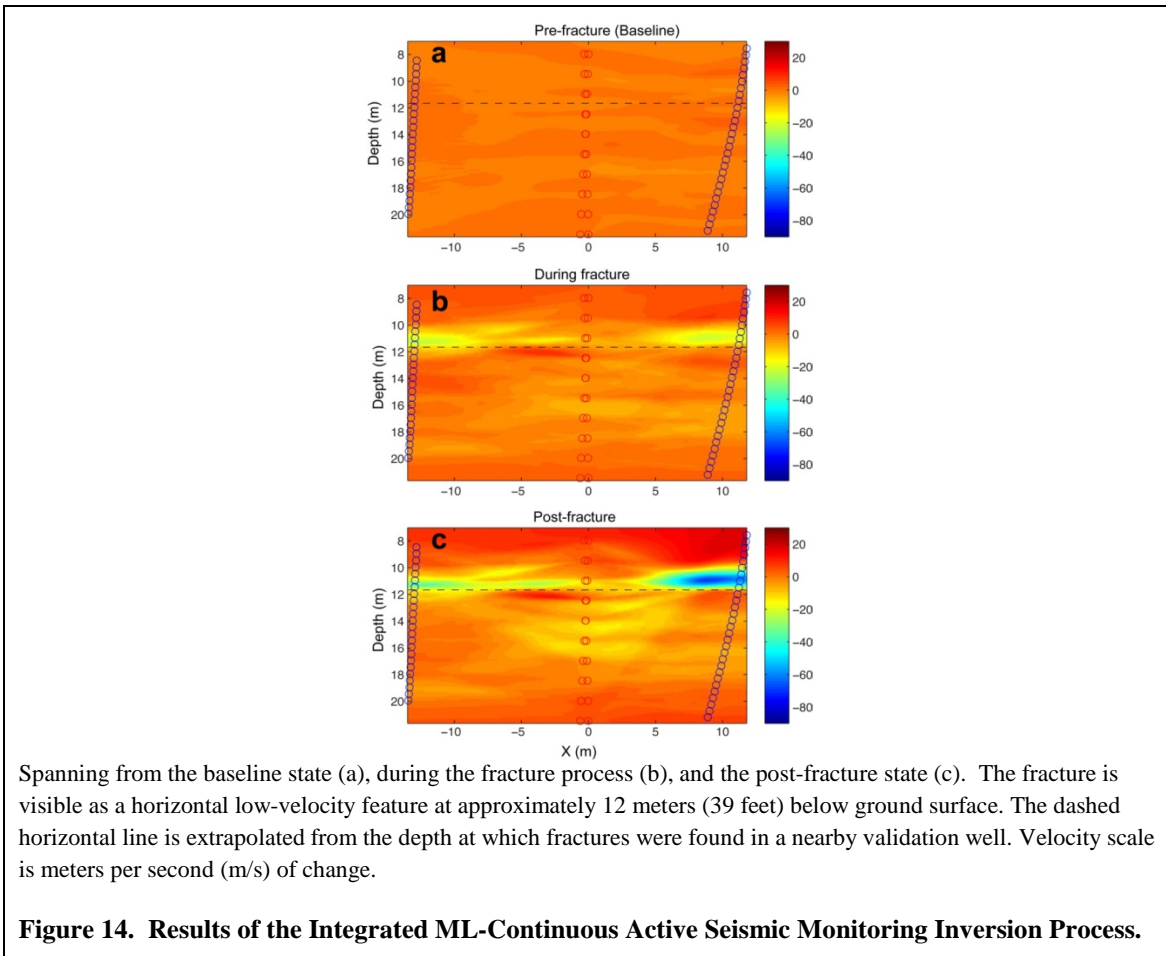
We found that the CASSM allowed for accurate, autonomous, and rapid monitoring of subsurface response to hydraulic fracturing. One advantage of the autonomous acquisition process is that no manual repositioning of sources or receivers is required; the static nature of the geometry guarantees excellent signal repeatability which simplifies extraction of subsurface changes. Figure 13 illustrates the changes in seismic velocity over time between two wellbores as a fracture is initiated nearby and as it propagates into the imaging plane. The decrease in velocity is what is expected as the rock loses strength, or becomes fractured. Figure 14 shows

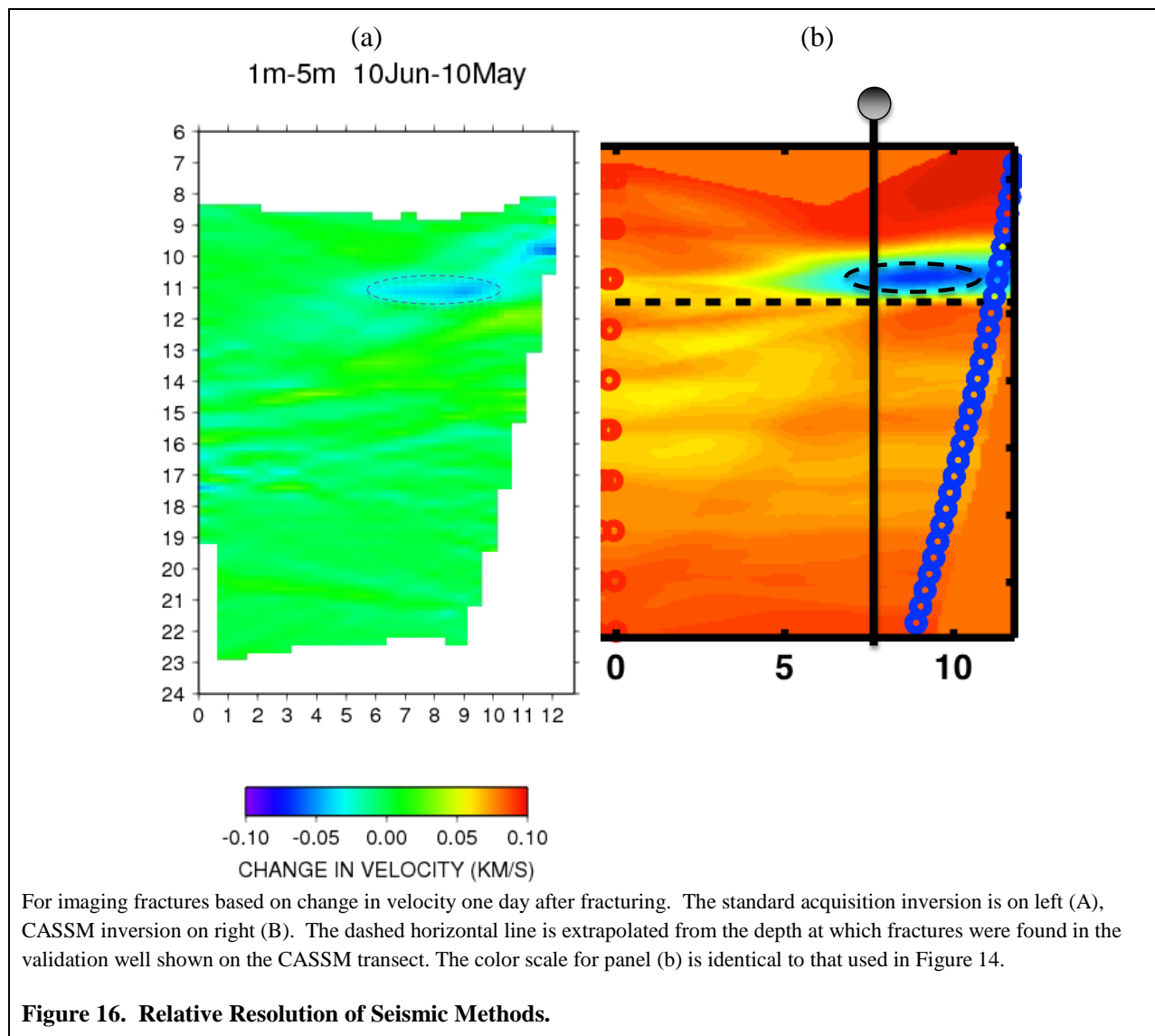
the change in velocity estimated using the CASSM approach along two imaging planes, which have been unfolded from 3 to 2 dimensions for enhanced visualization. Both of these figures show a clear decrease in velocity at approximately 12 m (39 ft) bgs which closely matches the fracture initiation depth recorded in the drilling log.



The high-resolution crosswell seismic velocity tomograms also revealed that there was an immediate decline in seismic velocity and that these data could be used to map the location and extent of the induced fractures. Figure 15 shows the change in seismic velocity along three transects 1 week after fracture installation using the standard tomographic seismic approach. As with the CASSM imaging, the standard seismic tomographic data revealed the presence of an interpreted fracture associated with the shallow installation, but not with the deeper fracture.

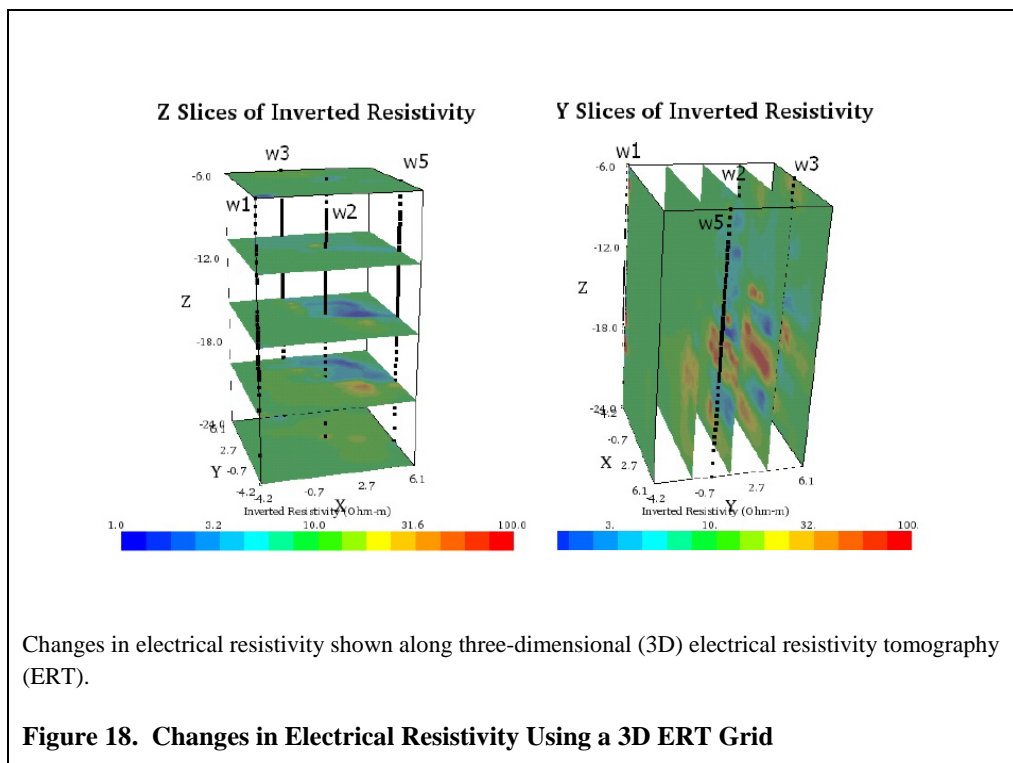
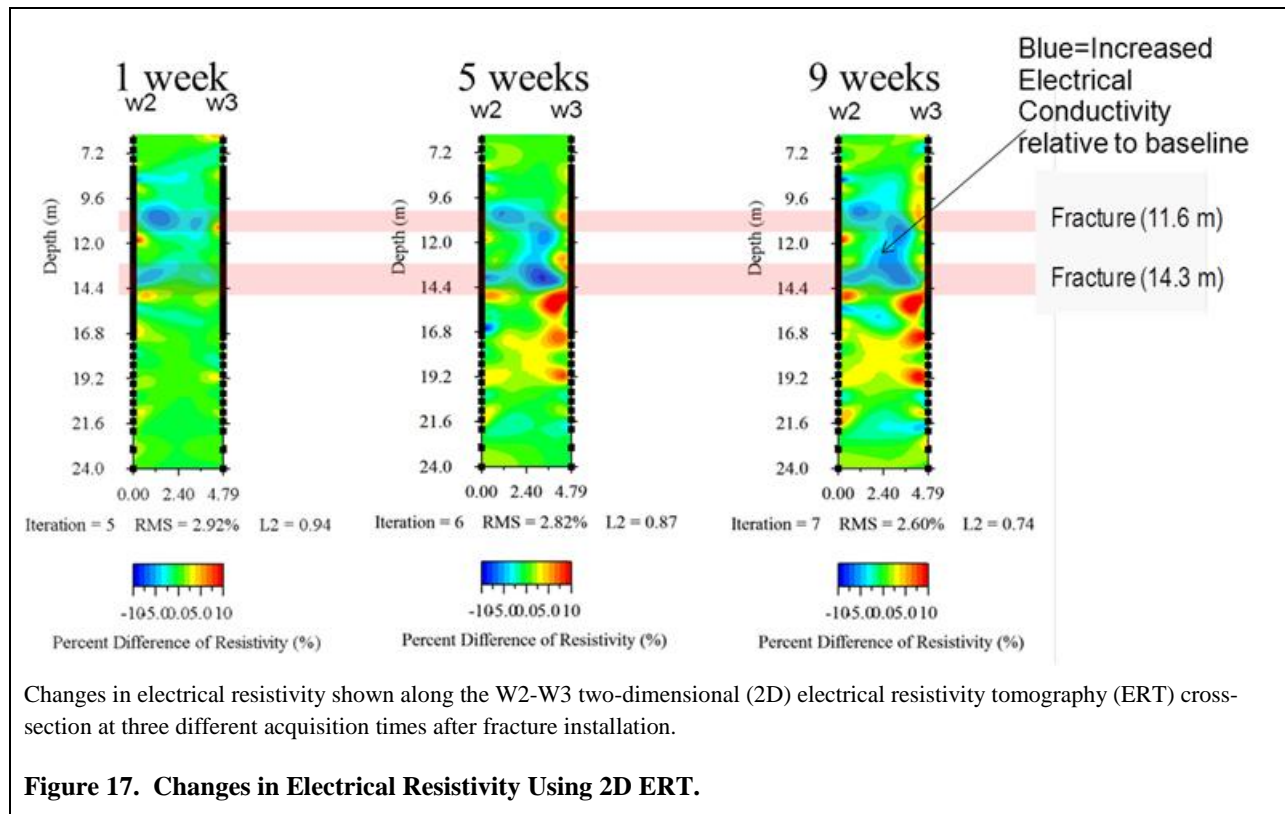
To evaluate the accuracy of both standard tomographic and CASSM for monitoring fracture emplacement, it is necessary to compare the geophysical responses with each other and with direct measurements of the fracture locations. Figure 16 shows the change in velocity due to the fracturing, obtained from the standard and CASSM seismic approaches. The oval indicates the location of the largest velocity anomaly, which indicates a decrease in velocity over time. The dashed line is a horizontal extrapolation of the base of an induced fracture, as identified from core samples retrieved from the borehole (drill back validation holes are described below). Figure 16 suggests that while both high resolution seismic methods were able to accurately image the location of the induced fracture (which is the ultimate goal of the project), the CASSM detection of the fracture location was superior due to high repeatability and low error (the latter was largely associated with stationary sensor positioning within the wellbore). However, the standard seismic tomograms provided higher spatial resolution and more spatial coverage compared to CASSM, and because they were collected over a longer period of time, also revealed fracture “healing” (not shown).





An increase in electrical conductivity was observed in conjunction with both the shallower and deeper fracture over time. Figure 17 shows an example of these changes along a two-dimensional (2D) ERT cross section and Figure 18 shows an example using a three-dimensional (3D) grid.

The greatest change in electrical conductivity occurred in the fractured region 2-3 months after fracturing. This delay in electrical response is consistent with the laboratory findings, where electrical conductivity increased most dramatically after breakdown of the guar. The 10-15% conductivity increase (resistivity decrease) in the shallower depth is also consistent with the core analysis described above. The change in conductivity in the deeper fracture indicates that while a complete fracture was likely not installed at this depth (as indicated by seismic and core), some porosity enhancement was produced by fracturing, which permitted the introduction of some amendment into the subsurface section.



The crosshole electrical data were useful for identifying distribution of the amendment injected within the induced fracture(s). These data showed that the radius of distribution of the geophysically-detectable injected amendment in the shallow fracture was substantially smaller than the fracture distribution itself. The ERT data also suggested that some amendment was injected into the deeper fracture initiation point, even if installation of a spatially extensive fracture was not successful. All data showed that the disturbed zone (through fracture creation or amendment injection) was offset from the fracture initiation point. We found that the 3D ERT data, which required substantially greater acquisition and inversion effort, did not add substantial value to interpretation of amendment distribution. Additionally, although surface ERT measurements were useful in delineating gross hydrogeological heterogeneities (e.g., water table, lithological units), the time-lapse surface ERT data were not useful for monitoring amendment distribution associated with fracturing due to the lower resolution nature of the measurements and also because other factors (e.g., moisture changes in the shallower section due to rainfall) contributed to the geophysical responses over time.

5.4.3 Confirmation Soil Boring Drilling and Core Analysis

Four confirmation soil borings were drilled near the fracture initiation point after fracture emplacement to evaluate if the fracture characteristics (e.g., fracture thickness and approximate extent) and amendment distribution assumed for the design were attained. These soil borings were collected in May 2011, approximately 1 year after fracture initiation.

Observations of the soil borings indicated the presence of fracture sand at location LBNL-2011-SB04 at approximately 10.7 m (35 ft) bgs, which correlates well with the shallow target depth. Location LBNL-2011-SB04 is approximately 8.8 m (29 ft) from the fracture initiation point (Figure 20). Odor and the presence of a pink/orange coloration were also observed at approximately 11 m (36 ft) bgs indicating the potential presence of amendment. Reddish striations were observed at soil boring location LBNL-2011-SB02 at a depth of approximately 11 m (36 ft) bgs. Fracture sand and odor were not observed at that location. Soil boring location LBNL-2011-SB02 is approximately 5.2 m (17 ft) from the fracture initiation point. Fracture sand and coloration were observed at soil boring location LBNL-2011-SB01 at approximately 11.9 m (39 ft) and 12.5 m (41 ft) bgs, respectively. Coloration was also observed at approximately 15.8 m (52 ft) bgs; however, no fracture sand was noted. This depth is slightly deeper than the intermediate target depth and is the only indication of potential fracture propagation and amendment distribution. Location LBNL-2011-SB01 is approximately 3.0 m (10 ft) from the fracture initiation point. Soil boring LBNL-2011-SB03 was cored but not logged. Overall, the 2011 confirmation soil boring data indicated a potential fracture radius of influence (ROI) up to 7.6 m (25 ft). Soil boring observations were recorded and are summarized in Appendix D.

Analysis of the core data suggests that geology may have impacted fracture propagation. According to the soil borings, fractures tended to propagate further in stiffer, more brittle clays as observed in the shallow groundwater zone near LBNL-2011-SB04. However, fracture propagation appeared to be inhibited by highly plastic, silty, clayey materials observed in the intermediate depths. It is assumed that the fracture propagated up into the shallow zone fracture following a path of least resistance.

To help understand the diffusion process of the injected amendment into the formation following fracture installation, sediment samples were collected from 6 inches above and below the fractures at both SB01 and SB03 for total organic carbon (TOC) analysis using a Shimadzu total inorganic carbon (TIC)/TOC analyzer at LBNL. Subsamples were taken for every 1/2 inch for

the first 2 inches and then every inch for another 4 inches both above and below the fracture aperture. For SB03, the fracture sand itself was also sampled due to its abundance. The sampling locations and concentrations of TOC for SB03 are shown in Figure 19. TOC concentrations are below the detection limit (<0.002%) for most samples from SB01, while detectable amounts of TOC were measured from samples from SB03. Compared to SB03, where fracture is apparent and large (Figure 19), only a thin fracture line was identified for SB01, indicating this may be the distal end of the fracture with limited organic carbon content. This is consistent with geophysical estimation of the fracture extension shown in Figure 20.

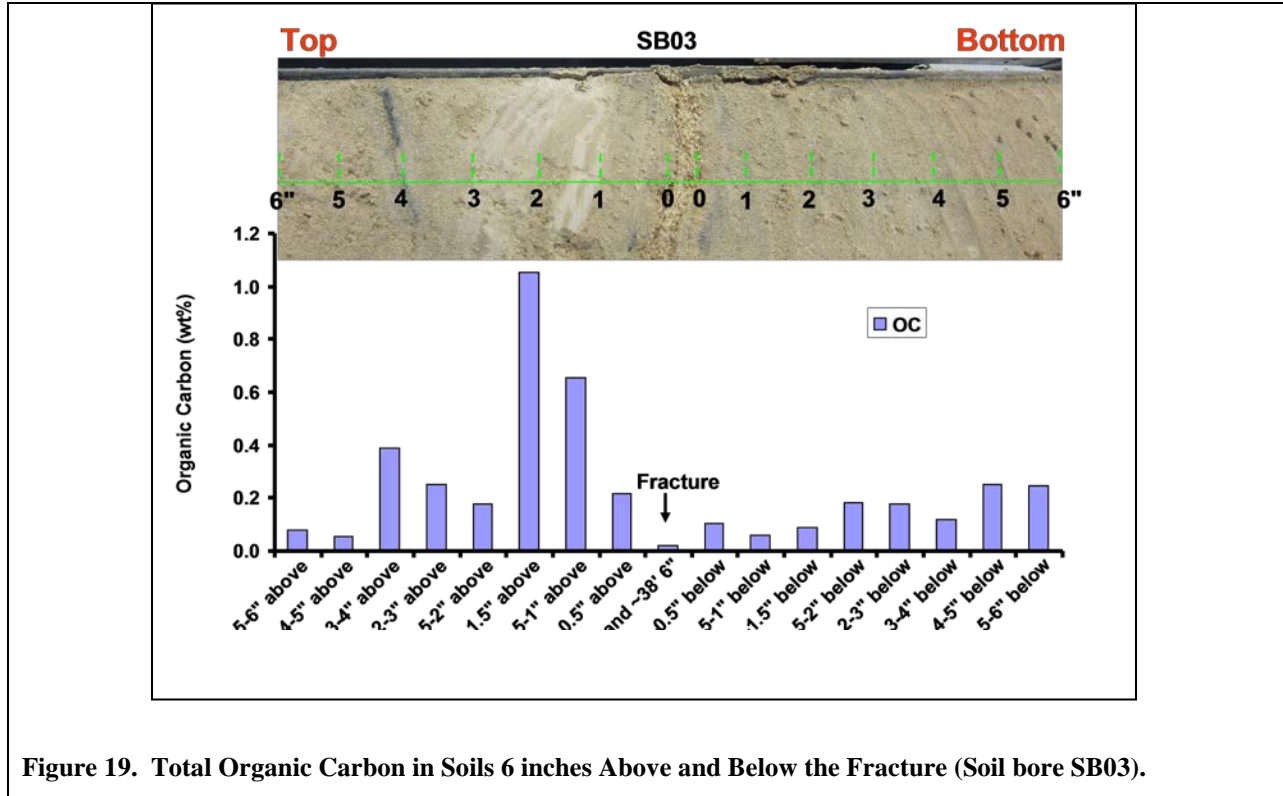
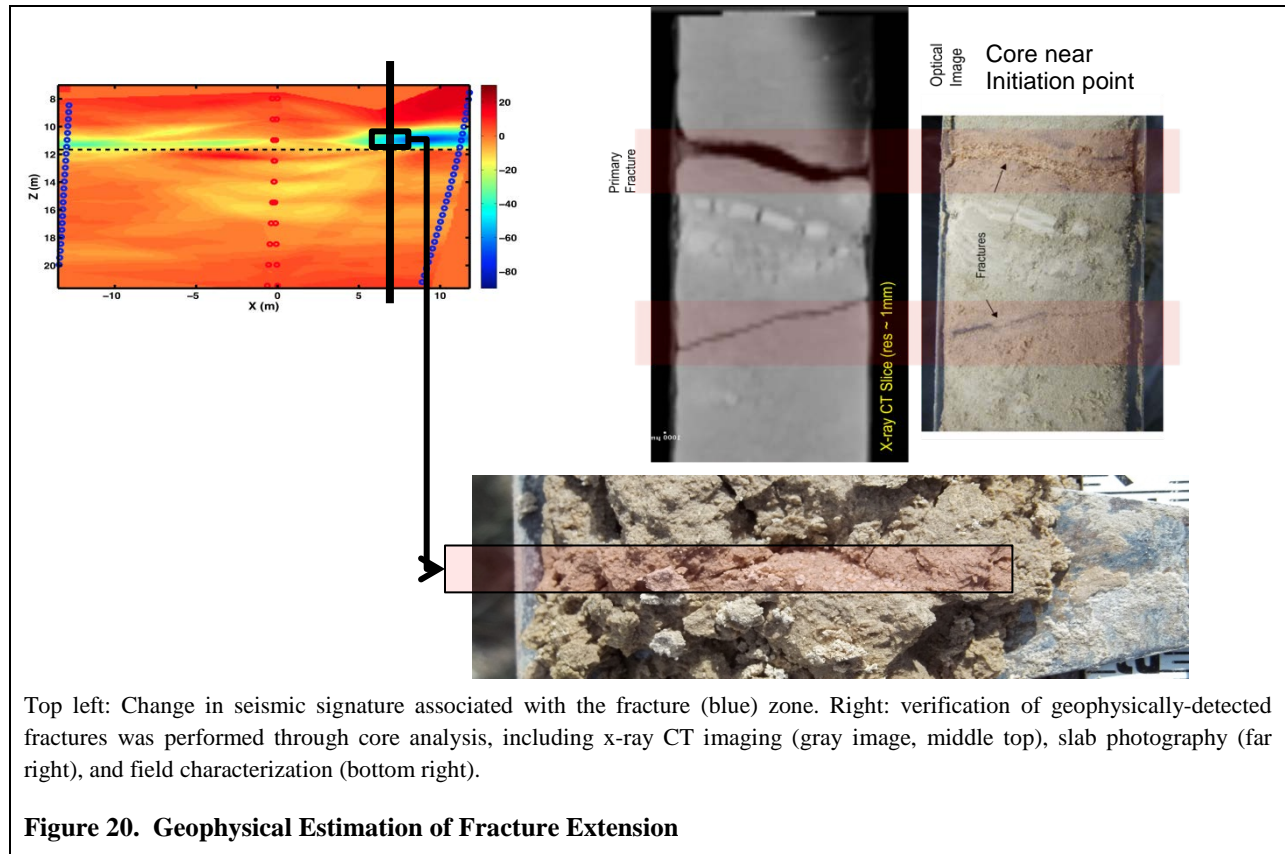


Figure 19. Total Organic Carbon in Soils 6 inches Above and Below the Fracture (Soil bore SB03).

Figure 19 shows that TOC concentrations range from 0.06 to 1% for soil samples from above and below the fracture and TOC concentration for the fracture sand itself is at 0.02%. The low TOC concentration of the fracture sand indicates the diffusion of organic carbon into the formations. While quantitative evaluation of the diffusion cannot be obtained because of the lack of measured background organic carbon concentrations in the soil before fracture installation and HRC[®] injection, TOC concentrations from soils above and below the fracture indicate the occurrence of diffusion following initial injection.



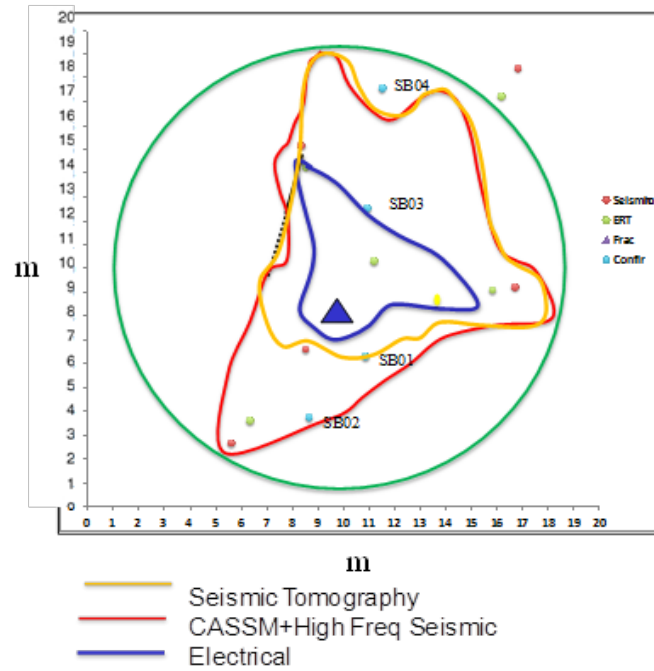
5.4.4 Geophysical Data Interpretation

The seismic, electrical, and validation core data were used to interpret the fracture locations as described above. The seismic tomography, CASSM, and ERT data agreed with the confirmation soil boring data for locations LBNL-2011-SB02 and -SB04; an example of this comparison is shown in Figure 20. Based on such validation, the geophysical data were used to interpret the spatial distribution of the fractures and amendments.

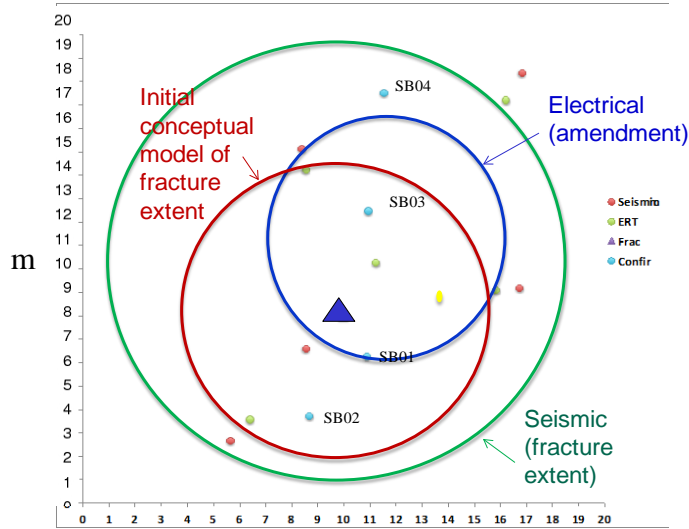
Figure 21(a) shows the interpreted outline of the fracture and amendment-impacted regions near the shallow fracture based on our developed geophysical signature understanding. The amorphous outlines indicated distributions based on the geophysical data over the regions where those data were collected. The green circle shows the estimated distribution of the fracture if the wellbore geometry had permitted imaging over all regions, based on connecting the farthest points of fracture disturbance that was geophysically detected. This “green circle” assumption has potential for both over and underestimation. The fractures may not have propagated where the geophysical data did not image (thus leading to an overestimation of the fracture disturbance area). However, it is also likely that the fractures continue at distances beyond those indicated by the geophysical data, based on limited geophysical detectability of small fractures (thus leading to an underestimation in the fracture disturbance area).

Figure 21(b) shows the interpreted distributions based on the assumption that the fractures and amendments are both radially distributed. It illustrates that the estimated fracture radius is greater than the initial conceptual model (shown by the red circle) and is offset, and that the estimated amendment lateral distribution is less than the initial conceptual model (which was equal in extent to the fracture distribution). Not shown but interpreted from the ERT data, is the

vertical extent of the amendment distribution, which was greater than the initial conceptual model. The figure shows that the centers of the fracture and amendment distribution regions were offset from the fracture initiation point. The combined ERT and seismic data suggest that although a good fracture was not successfully installed in the deeper zone, some porosity enhancement occurred, which enabled the introduction of some amendment into that zone.



(a)



(b)

Top: Distribution of fractures and amendments based on geophysical data (yellow, red, and blue outlines), only considering the regions over which seismic data were collected. The green circle indicates the distribution of the installed fracture by assuming that the fracture is radially distributed over the areas that the geophysical data could not image due to borehole geometry. The blue line indicates the distribution of amendment within the fracture, based on electrical resistivity tomography (ERT). Bottom: A comparison of the estimated fracture distribution from the geophysical data (green circle, assuming radially distributed) with the distribution used to guide remediation at Spill Site 7 (red circle) and the amendment distribution from ERT (blue).

Figure 21. Interpreted Fracture and Amendment Distributions

SECTION 6 – PERFORMANCE ASSESSMENT

As previously stated, the primary objective of this project is to assess the utility of surface and crosshole geophysical methods for developing a conceptual model of amendment distribution via hydraulic fracturing. Accomplishing this objective is dependent on the quantitative and qualitative performance objectives described below.

6.1 Quantitative Performance Objectives

The success of the demonstration is dependent on four quantitative performance objectives: 1) confirm fracture characteristics, 2) quantify utility of geophysical methods for delineating fracture and HRC[®] ROI, 3) assess the value of different geophysical approaches, and 4) determine if there is a cost benefit. These objectives are listed in Table 1 and are described below.

6.1.1 Quantitative Objective #1

The first objective (confirmation of fracture characteristics) was assessed by evaluating post-fracture installation soil cores to observe fracture characteristics including physical ROI, fracture thickness, and presence of HRC[®] within the fracture. A physical fracture radius of 7.0 m (23 ft) from the initiation borehole with 2,000 pounds installed per fracture was observed. Based on the success criteria listed in Section 3, an observed direct correlation between SS7 and Plume E was achieved.

6.1.2 Quantitative Objective #2

This objective focused on interpretation of the geophysical datasets in terms of the mean radius and variance of the radius of the fractures and HRC[®] from the injection point as a function of heterogeneity. The data required to assess this criteria includes the inverted time-lapse field geophysical datasets, interpreted with consideration of the laboratory experimental results and validated using the confirmation soil core information as is shown in Figure 21. This objective was partially achieved. Different individual geophysical datasets were used to estimate the mean horizontal distribution of the fractures (between 7.0 and 9.1 m [23 and 30 ft]), and combinations of data were also used to increase confidence in the interpretation. ERT data were used to estimate the vertical and mean radius (5.2 m [17 ft]) of injected amendment. However, because different geophysical datasets offered different quality of information (refer to Section 6.1.3), we choose to use a scenario approach for input to the cost-benefit analysis rather than estimating a variance associated with a single measurement approach only.

6.1.3 Quantitative Objective #3

This objective focuses on assessing the value of different geophysical approaches for guiding development of amendment delivery strategy. As indicated in Table 5, comparison of geophysical data with wellbore validation data allowed us to assess the relative value of the different approaches for monitoring fractures and amendment. The high frequency tomographic and CASSM methods were most useful for identifying the fracture characteristics (spatial distribution and fracture propagation details, respectively), while the 2D crosshole ERT were most useful for providing information about amendment distribution.

Table 5. Summary of Geophysical Method Performance

	Method	Hypothesis	Detection?	Utility?
Seismic	High-frequency P-wave seismic ★	Decrease in Vp, Increase in 1/Qp	Decrease in Vp clear, artifacts exist	Spatial distribution of fractures
	ML-CASSM ★	Decrease in Vp, Increase in 1/Qp	Decrease in Vp, small increase in attenuation	Fracture propagation detail
Electrical	Surface ERT ~	Increase in conductivity	Time-lapse corrupted by changes in soil moisture (etc)	Not useful for monitoring but useful for baseline characterization
	Borehole ERT (2D) ★	Increase in conductivity	Decrease in resistivity, some anomalies	Amendment distribution
	Combined 3D ERT ~	Increase in conductivity	Decrease in resistivity, some anomalies.	Amendment distribution

Notes:

The red stars indicate the methods that were deemed to be most useful for monitoring the fracture emplacement and subsequent amendment distribution.

2D = two-dimensional

3D = three-dimensional

ERT = electrical resistivity tomography

Qp = Seismic P-wave quality factor (inverse of attenuation)

Vp = Seismic P-wave velocity

Quantitative performance success is dependent on whether the use of geophysics can reduce the number of fracture initiation points by 20%. The value-added in the use of geophysical methods was evaluated by assessing/comparing two situations. The first situation considers only historical site data and soil boring data, and the second situation evaluates the use of the geophysics datasets.

Although fracture ROIs have been observed to vary somewhat across FEW, soil cores collected from SS7 and other FEW plumes indicated that 2,000 pounds of proppant material reproducibly creates fractures with radii of approximately 5.2 to 7.0 m (17 to 23 ft) from the initiation point, or an average of a 6.1-m (20-ft) physical fracture radius. Based on the field-scale pilot tests conducted at both SS7 and Zone C, a 6.1 m (20 ft) ROI was chosen as the standard design for the demonstration site (Plume E). Two scenarios were evaluated for this performance and cost assessment, a conservative ROI of 7.0 m (23 ft) and the more probable ROI of 7.6 m (25 ft). Scenario 1 and 2 were evaluated for four different treatment zone areas (1, 4, 8, and 20 acre sites) and compared to the standard design ROI of 6.1 m (20 ft). For each treatment zone area, the number of initiation points was determined for each ROI by dividing the total treatment zone area by the impact area associated with the ROI assuming a circular distribution. The % difference between the standard design and the Scenario 1 and 2 designs was then calculated. Results for both scenarios are included in Table 6 and Table 7.

Both Scenarios 1 and 2 achieved at least a 20% reduction in the number of fracture initiation points as required by the performance criteria.

Table 6. Performance Evaluation: Scenario 1

Treatment Zone (acres)	1.0	4.0	8.0	20.0
Number of Initiation Points (20 ft ROI)	35	139	277	694
Number of Initiation Points (23 ft ROI)	27	109	217	544
% Difference (Decrease)	-21.6%	-21.6%	-21.6%	-21.6%

ft = feet
ROI = radius of influence

Table 7. Performance Evaluation: Scenario 2

Treatment Zone (acres)	1.0	4.0	8.0	20.0
Number of Initiation Points (20 ft ROI)	35	139	277	694
Number of Initiation Points (25 ft ROI)	22	88	175	438
% Difference (Decrease)	-36.8%	-36.8%	-36.8%	-36.8%

ft = feet
ROI = radius of influence

6.1.4 Quantitative Objective #4

The cost-effectiveness of geophysical imaging relies upon both the cost of technologies used and quality of data obtained. The cost-benefit analysis included: 1) interpretation of qualitative and quantitative performance objectives using integrated geophysical and soil core sample analysis; 2) cost of the dynamic pilot test and associated interpretation; and 3) actual costs associated with the SS7 full-scale RA using a design strategy based on conventional soil core- and groundwater monitoring-based methods alone. Based on the SS7 remedial design and potential treatment zone size, the number of installed fractures was estimated for both Scenarios 1 and 2 for each evaluated treatment zone area. Using a per fracture cost developed from the actual SS7 RA cost, the total cost of implementation was estimated and compared to the cost of the standard design. For Scenario 1, geophysics is only a viable option for larger sites, greater than 20 acres. For Scenario 2, geophysics was found to be viable for treatment zone areas greater than 4 acres. Complete results, further details, and assumptions relating to the cost benefit are included in Section 7.

6.2 Qualitative Performance Objectives

The success of the demonstration is dependent on four qualitative performance objectives, which are to 1) determine which geophysical method provides the best information about fracture delineation, 2) determine which geophysical method provides the best information about HRC[®] distribution, 3) determine which geophysical datasets are optimal for monitoring both fracture

creation and HRC[®] distribution, and to 4) assess field ruggedness, required user experience, and overall signal-to-noise ratio of commercially available geophysical approaches for monitoring HRC[®] and fracture distribution.

6.2.1 Qualitative Objective #1

After a careful examination of the acquired datasets, the two modalities of high-frequency time-lapse seismic datasets were deemed to provide the best information concerning fracture location. Both the P-wave seismic and CASSM acquisition methods located and spatially mapped the upper fracture zone; estimated fracture depths matched well with both drilling logs from fracture emplacement and fracture location estimated from confirmation boreholes. While both seismic acquisition methods provided equivalent results in the post-fracture period, the CASSM dataset provided both better time resolution during the fracturing process and more repeatable waveforms; this combination of factors increased our confidence during the interpretation process.

6.2.2 Qualitative Objective #2

Despite the success of the seismic imaging approaches in determining the fracture locations, neither interpreted seismic dataset (seismic velocity or attenuation alteration) provided definitive information concerning HRC[®] distribution within the emplaced fracture. This is not surprising considering that the seismic response is due to mechanical alteration (introduction of the fracture/proppant system) and the fluid added to the proppant is probably a secondary effect. The most informative dataset for estimating HRC[®] distribution appeared to be the borehole ERT dataset, which effectively captured the guar breakdown process and HRC[®] diffusion into the formation.

6.2.3 Qualitative Objective #3

No single geophysical technique allowed simultaneous mapping of both fracture extent and amendment distribution with a high degree of confidence. This observation suggests that multi-method acquisition would be the most effective approach for achieving this qualitative objective. Considering that both borehole ERT and seismic instrumentation can be effectively co-located in monitoring wells, a possible solution might be co-instrumentation with CASSM and borehole ERT to capture separate processes from a similar geometry. This seismic/ERT co-instrumentation approach is currently being adopted for deep monitoring systems used to map subsurface CO₂ movement (e.g. Hovorka et.al. 2011).

6.2.4 Qualitative Objective #4

Of the techniques evaluated, borehole ERT is the most mature when applied to environmental monitoring tasks. Commercial vendors can supply the acquisition electronics and turn-key processing packages allowing wide deployment of the technique with minimal training required. Campaign high-frequency seismic acquisition systems are also available commercially but are somewhat more complicated to deploy; also, a key component of the data processing flow (travel-time picking) is a manual process and requires a reasonable degree of training to effectively perform. The CASSM technique, while robust, is currently not commercially available as a system although the majority of the components can be purchased from commercial sources. The processing of CASSM datasets is also more time consuming due to the

large data volume of a typical acquisition run (orders of magnitude larger than traditional campaign seismic acquisition). At the present time, a combination of borehole ERT and campaign high-frequency seismic acquisition may be the best choice considering training and equipment requirements; however, the CASSM system utilized in this project would be relatively straight-forward to commercialize (both acquisition and processing), a process which make this technique available to a broader community.

SECTION 7 – COST ASSESSMENT

7.1 Cost Model

A cost model for the use of geophysical imaging to investigate the delivery of amendments in the subsurface is provided in Table 8. The table identifies specific cost elements, the data tracked corresponding to the cost elements, and the associated costs. Because this demonstration is based, in part, on the SS7 RA, the actual costs for implementing the RA are also included.

In developing the cost model, it was assumed that only the drilling, biostimulation, and bioaugmentation cost elements were impacted by a change in ROI, and therefore, the number of fracture initiation points. In Table 8, the drilling, biostimulation, and bioaugmentation costs to implement the geophysical methods are presented on a cost per fracture basis. Drilling costs include the drilling subcontractor, IDW disposal, surveying, and labor; prorated based on the number of new monitoring wells and confirmation soil borings installed in each groundwater zone. Biostimulation costs include subcontractors and materials (HRC[®], fracture sand, guar, and other fracturing related materials), equipment rental, and labor associated with hydraulic fracturing activities. Biostimulation costs are prorated based on number of fracture initiation locations installed in each groundwater zone. Bioaugmentation activities costs include the pneumatic injection subcontractor, microbial culture materials (e.g., KB1[™]), and labor; prorated based on the number of bioaugmented injection wells in each groundwater zone.

Certain cost elements in the cost model are assumed to be constant for a full-scale implementation and not dependent on changes in fracture ROI. These cost elements include the remedial design, groundwater monitoring, project management, geophysical capital and labor, and site closure activities. These are reflected as “Non-Impacted Costs” in Table 8. Groundwater monitoring costs are prorated based on the number of performance monitoring wells in each groundwater zone.

Table 8. Cost Model

Cost Element	Data Tracked	Estimated Cost
Actual Costs to Implement Full-Scale RA at FEW SS7 - Shallow GW Zone		
Remedial Design**		\$ 596,325.00
Drilling Activities*	Monitoring Well Installation	\$ 11,645.50
	Confirmation Soil Borings	\$ 55,882.50
	Investigation-Derived Waste (IDW)	\$ 18,192.50
	Surveying	\$ 9,792.50
Groundwater Monitoring Activities	GW Monitoring	\$ 146,304.00
	Analytical Data Validation	\$ 8,487.00
	Monitoring Report	\$ 15,028.00
Biostimulation Activities*	Mobilization/Demobilization	\$ 46,406.50
	Fracturing (Sub and Materials)	\$ 1,381,673.50
	Remedial Action Report	\$ 32,065.50
	ERPIMS, Database, GIS	\$ 6,018.50
Bioaugmentation Activities*	Remedial Design Update	\$ 33,704.00
	Pneumatic Injection (Sub and Materials)	\$ 177,031.00
Project Management Activities	Project Management	\$ 107,337.00
	Meetings	\$ 33,200.00
Site Restoration and Close-Out**		\$ 28,553.00
Total (Shallow GW)		\$ 2,707,646.00
Estimated Costs to Implement Geophysical Methods		
Remedial Design**		\$ 596,325.00
Geophysics (CASSM)	Capital Costs, labor, mobilization, data interpretation	\$ 104,000.00
Drilling Activities* per Fracture	Monitoring Well Installation	\$ 18.22
	Confirmation Soil Borings	\$ 87.45
	Investigation-Derived Waste (IDW)	\$ 28.47
	Surveying	\$ 15.32
Groundwater Monitoring Activities	GW Monitoring	\$ 146,304.00
	Analytical Data Validation	\$ 8,487.00
	Monitoring Report	\$ 15,028.00
Biostimulation Activities* per Fracture	Mobilization/Demobilization	\$ 72.62
	Fracturing (Sub and Materials)	\$ 2,162.24
	Remedial Action Report	\$ 50.18
	ERPIMS, Database, GIS	\$ 9.42
Bioaugmentation Activities* per Fracture	Remedial Design Update	\$ 52.74
	Pneumatic Injection (Sub and Materials)	\$ 277.04
Project Management Activities	Project Management	\$ 107,337.00
	Meetings	\$ 33,200.00
Site Restoration and Close-Out**		\$ 28,553.00
Total Per Fracture Cost*		\$ 2,773.73
No. of Fractures		1
Non-Impacted Costs (Shallow GW)		\$ 1,039,234.00
Total (Shallow GW)		\$ 1,042,007.73

Notes:

*Activities impacted by number of fracture initiation points.

**Cost included based upon Final Record of Decision (ROD), 2006

7.2 Cost Drivers

Potential cost drivers that should be considered when selecting geophysical imaging for developing a conceptual model of fracture propagation and amendment distribution include the size of the treatment area and site geology.

When using geophysical methods like CASSM, the cost to purchase the necessary equipment can be a large percentage of the implementation cost, especially for smaller treatment zones. As shown in this demonstration, geophysical imaging was not a financially viable option for 1-acre treatment sites. Financial practicality at average-sized sites (e.g., 4 to 8 acres) was dependent on the potential fracture impact area which may be influenced by geology.

As described in Section 5, site geology may impact fracture propagation, and therefore, treatment success. The use of geophysical methods can help identify fracture installation and confirm or supplement soil boring observations early in the remediation process. For this study, the intermediate aquifer zone fracture did not propagate as expected and instead may have moved up into the shallow fracture following a path of least resistance. The use of geophysical methods identified this issue early on. If implemented during a field-scale RA, early identification can allow for timely corrective actions to ensure effective treatment and potentially reduced risk of remediation failure or additional costs.

7.3 Cost Analysis

Since the cost-benefit analysis for development of an amendment delivery strategy using geophysical data is based on the implemented SS7 full-scale RA, it was important that the pilot test be as similar as possible to the RA implemented at SS7. To document fracture characteristics for comparison to other FEW areas, each fracture was evaluated using traditional confirmation soil boring methods and compared to previously collected data. Soil cores collected from SS7 and other FEW plumes indicated that 2,000 pounds of proppant material reproducibly creates fractures with radii of approximately 5.2 to 7.0 m (17 to 23 ft) from the initiation point, or an average of a 6.1-m (20-ft) physical fracture radius. As stated in Section 6, a 6.1 m (20 ft) ROI was chosen as the standard design for comparison to geophysical methods at Plume E. The pilot test was designed with geophysical data wells installed to image fractures with a radius of 4.6 to 9.1 m (15 to 30 ft) from the initiation point.

Using the actual RA costs from SS7 (Table 8), a per fracture cost was estimated to be \$2,774. It was assumed that the site geology was consistent throughout the entire treatment zone, regardless of size. This assumption limited the number of pilot tests to one, and therefore, one unit cost for geophysical methods. Because the cost analysis was evaluated using a per fracture cost, another assumption was that the fracture implementation would be similar to the remedial design for SS7. For example, at SS7 each fracture initiation point had 4, 5, or 6 fractures installed. Within the 400 parts per billion (ppb) contour of SS7, 37.5% of the fracture initiation points had four fractures, 25% had five fractures, and 37.5% had six fractures. This same methodology was used for each treatment zone area evaluated to determine the total number of fractures installed. It was also assumed that, based on the CASSM and ERT dataset results, only CASSM would be chosen for use during a field-scale pilot test. Amendment is not likely to distribute laterally beyond the fracture. Based on the success at SS7, it is anticipated that the bacteria will grow, or “bloom,” away from delivery zones as aquifer conditions are established by migrating amendment materials, potentially creating bioactivity zones between delivery points over time.

In situ bioremediation application, such as the RA implemented at SS7, have excelled in fine-grained, slow moving groundwater conditions where hospitable geochemical conditions (e.g., adequate and available food source) have been established, with native microbes “blooming” up to 21.3 m (70 ft) from amendment delivery locations. For this reason, it is anticipated that geophysical imaging of the fracture propagation is sufficient for remedial design purposes, and therefore, only CASSM costs were incorporated into the cost analysis.

Results of the cost-benefit analysis for Scenarios 1 and 2 are included in Table 9 and Table 10, respectively.

Table 9. Cost-Benefit Analysis: Scenario 1

Treatment Zone Area Size	1 acre	4 acres	8 acres	20 acres
Number of Fractures - 20 ft ROI	173	694	1,387	3,468
Estimated Cost - 20 ft ROI	\$480,986	\$1,923,942	\$3,847,885	\$9,619,712
Number of Fractures - 23 ft ROI	136	544	1,087	2,718
Estimated Cost - 23 ft ROI	\$480,961	\$1,611,844	\$3,119,689	\$7,643,222
% Cost Savings	0.0%	-16.2%	-18.9%	-20.5%

ft = feet

ROI = radius of influence

Table 10. Cost-Benefit Analysis: Scenario 2

Treatment Zone Size	1 acre	4 acres	8 acres	20 acres
Number of Fractures - 20 ft ROI	173	694	1,387	3,468
Estimated Cost - 20 ft ROI	\$480,986	\$1,923,942	\$3,847,885	\$9,619,712
Number of Fractures - 25 ft ROI	110	438	876	2,190
Estimated Cost - 25 ft ROI	\$407,775	\$1,319,101	\$2,534,202	\$6,179,505
% Cost Savings	-15.2%	-31.4%	-34.1%	-35.8%

ft = feet

ROI = radius of influence

From these results, it is evident that for Scenario 1 (7 m [23 ft] ROI), the use of geophysics to achieve a 20% cost savings is only a viable option for larger sites (greater than 20 acres). For Scenario 2, (7.6 m [25 ft] ROI), the use of geophysics to achieve a 20% cost savings was found to be viable for treatment zones greater than 4 acres, generating a cost savings greater than 30% for the three treatment zone sizes evaluated.

Due to similar site lithology and contaminant distribution, it is anticipated that Plume E will be impacted by the implemented RAs the same way as SS7. As identified in the Record of Decision (ROD), the timeframe for SS7 to meet RAOs is estimated at 35 years for the shallow aquifer zone and 175 years for the intermediate aquifer zone (USAF 2006a). As of the March 2009 performance monitoring conducted at SS7, the updated groundwater model results indicate that MCLs may be reached in the shallow aquifer zone approximately 25 to 30 years after

bioremediation initiation. Considering bioremediation was initiated in 2006, MCLs in the shallow aquifer zone are estimated to be reached in 2036 or 2037. The model indicates that MCLs may be reached in the intermediate aquifer zone 50 to 55 years after bioremediation initiation, or in 2061.

SECTION 8 – IMPLEMENTATION ISSUES

There are several issues that could potentially impact the use of geophysical data to provide high-quality data needed to design a full-scale remedial treatment. The first issue is the thoughtful design of the pilot study site, which should take into consideration the (often limited) propagation characteristics of the different geophysical signals, expected fracture distribution and costs of drilling wellbores for geophysical data acquisition. Not surprisingly, our demonstration found that we could estimate with high confidence the fracture and amendment distribution where wellbore placement resulted in good geophysical signal coverage, but that our certainty was lower elsewhere. Although trade-offs between wellbore spacing, cost, geophysical coverage, and resolution cannot be circumvented, they do require thoughtful consideration during planning.

Another issue is the role of heterogeneity on fracture propagation characteristics. Our demonstration was designed to test and image induced fracture characteristics in two different lithologies. The geophysical data in fact illustrated that we were unsuccessful at installing fractures in one of the lithologies. Although these results highlight the value of geophysical monitoring for understanding fracture distribution as a function of heterogeneity, they also emphasize the need to also consider the geology carefully during pilot study and full-scale design of fracture-based treatment.

The last implementation issue we identified is related to the procurement of one of the geophysical methods tested in this demonstration. All but one of the methods are commercially available. However, the CASSM system was developed at LBNL, and therefore, is not commercially available. However, fabrication of the system is not onerous – it can be built by interested geophysical service providers and used to provide a unique and useful service. As such, we included the fabrication costs-benefit that involved the use of CASSM as a fracture monitoring tool.

SECTION 9 – REFERENCES

- Ajo-Franklin, Jonathan B., Burke J. Minsley, and Tom M. Daley 2007. Applying compactness constraints to differential travelttime tomography", *Geophysics*, Vol. 72, No. 4, p. R67-R75.
- Ajo-Franklin, J., T. Daley, B. Butler-Veytia, J. Peterson, Y. Wu, B. Kelly, and S.S. Hubbard 2011. Multi-level continuous active source seismic monitoring (ML-CASSM): Mapping shallow hydrofracture evolution at a TCE contaminated site. *SEG Expanded Abstract*, 30, Presented at the SEG Annual Meeting, San Antonio, TX, September 18–23, 2011.
- Daley, T.M., Solbau, R.D., Ajo-Franklin, J.B., and Benson, S.M. 2007. Continuous Active-Source Seismic Monitoring of CO₂ Injection in a Brine Aquifer: *Geophysics*, Vol. 72, No. 5, p. A57-A61.
- Daley, T., Ajo-Franklin, J.B., and C. Doughty, 2011. Constraining the reservoir model of an injected CO₂ plume with crosswell CASSM at the Frio-II Brine Pilot: *International Journal of Greenhouse Gas Control*, Vol. 5, No. 2, pp. 1022-1030.
- Hovorka, S.D., Meckel, T.A., Trevino, R.H., Lu, J., Nicot, J.P., Choi, J.W., Freeman, D., Cook, P., Daley, T.M., Ajo-Franklin, J.B., Freifeild, B.M., Doughty, C., Carrigan, C.R., La Brecque, D., Kharaka, Y.K., Thordsen, J.J., Phelps, T.J., Yang, C., Romanak, K.D., Zhang, T., Holt, R.M., Lindler, J.S., Butsch, R.J., 2011, Monitoring a large volume CO₂ injection: Year two results from SECARB project at Denbury's Cranfield, Mississippi, USA, *Energy Procedia*, Vol. 4, Pages 3478-3485.
- Hubbard, S.S., K. Williams, M. Conrad, B. Faybishenko, J. Peterson, J. Chen, P. Long and T. Hazen, Geophysical monitoring of hydrological and biogeochemical transformations associated with Cr(VI) Biostimulation, *Environmental Science and Technology*, DOI 10.1021/es071702s, 2008.
- Lawrence Berkley National Laboratory (LBNL). 2010. Demonstration Plan: Geophysical Imaging for Investigating the Delivery and Distribution of Amendments in the Heterogeneous Subsurface of the F.E. Warren AFB. February.
- Revil, A., and P.W.J. Glover. 1997. Theory of ionic surface electrical conduction in porous media. *Phys. Rev. B* 55:1757–1773.
- Revil, A. and P. W. J. Glover (1998), Nature of surface electrical conductivity in natural sands, sandstones, and clays, *Geophys. Res. Lett.*, 25(5), 691–694, doi:10.1029/98GL00296.
- United States Air Force (USAF). 2003. Final Zone D Groundwater Remedial Investigation Report. F.E. Warren Air Force Base, Wyoming. October.
- USAF. 2006a. Record of Decision, Zone D Groundwater, F.E. Warren Air Force Base, Cheyenne, Wyoming. July.
- USAF. 2006b. Final Zone D Source Areas Remedial Investigation Report, F.E. Warren Air Force Base, Cheyenne, Wyoming. July.

APPENDIX A
PHASE I LABORATORY EXPERIMENTS SUMMARY

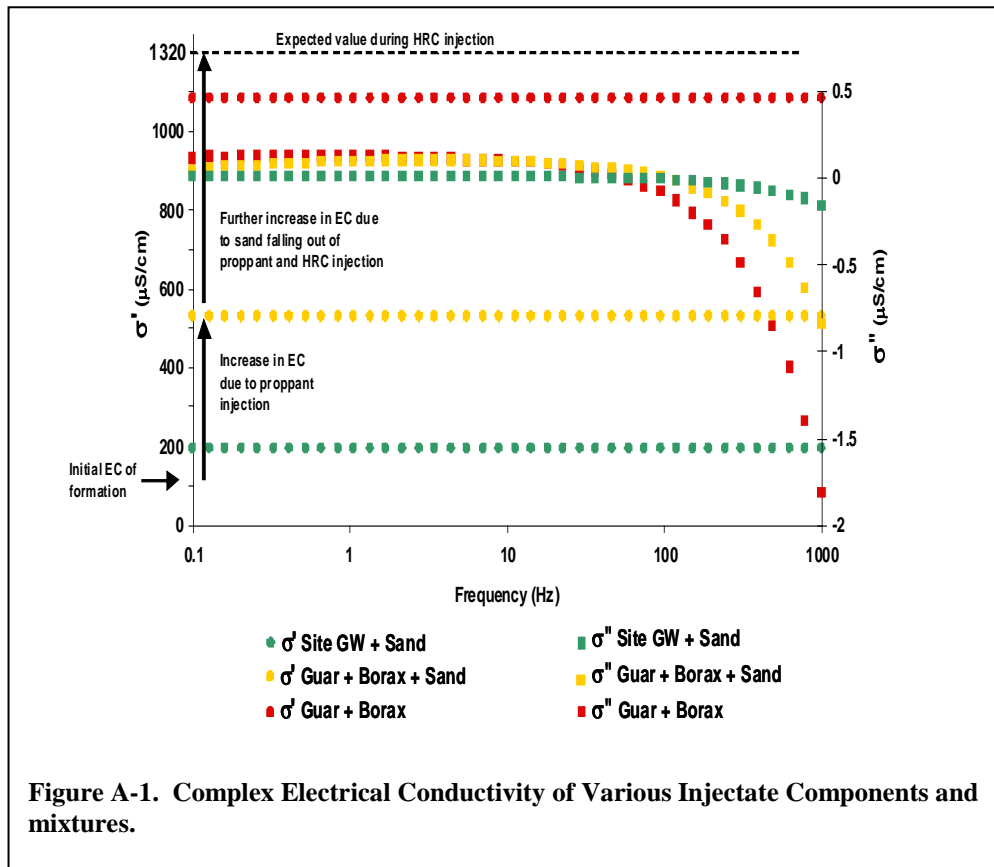
APPENDIX A – PHASE I LABORATORY EXPERIMENTS

Laboratory experiments (including batch and flow through columns) were used to determine the geophysical signatures of the different injectate components (HRC[®], sand proppant, borax and guar) as well as to their mixtures under different temperature conditions and concentrations. These experiments were used to test conceptual models about what we expected to be able to image in the field using geophysical approaches. A summary of the laboratory experimental results were included in the demonstration report and are summarized in this Appendix.

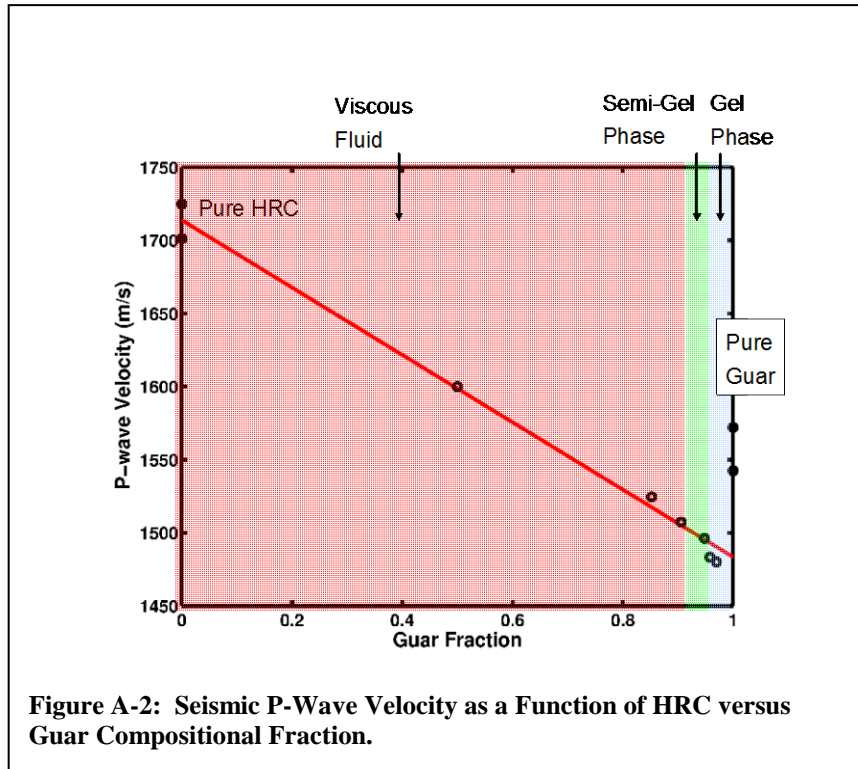
Electrical Resistivity

Over the expected concentration ranges expected to be encountered in the field, fluid batch experiments were performed to explore the electrical conductivity (EC) of the injectate components and mixtures. These experiments indicated the following relationship relative to site groundwater (790 micro Siemens per centimeter [$\mu\text{S}/\text{cm}$]) and saturated FEW site sediments ($\sim 100 \mu\text{S}/\text{cm}$).

$$EC_{\text{HRC}} > EC_{\text{Borax}} > EC_{\text{site groundwater}} > EC_{\text{Guar}} > EC_{\text{saturated formation}}$$



Column experiments were also performed to explore the electrical signature as HRC[®] is introduced into a guar-borax-sand slurry (Figure A-1). These experiments indicated that: the addition of HRC[®] to a guar-sand slurry caused the sand to quickly drop out of the slurry (within minutes), the temperature decreased slightly (as did the EC) after introduction of HRC[®], and that the guar degraded over time, which caused a slight decrease in EC. The electrical phase response to the injectate materials was found to be negligible.



Seismic Velocity

Instrumentation was developed and utilized to obtain measurements of seismic waveforms traveling through liquid and semi-solid samples at multiple offsets, which permits accurate estimates of the seismic velocity under different sample conditions. Measurements showed that the P-wave velocity of HRC[®] is approximately 1715 meters per second (m/s) and that guar gel in pure form had a P-wave velocity of approximately 1535 m/s, very close to liquid water. The P-wave velocity trend (from 100% HRC[®] to 100% Guar as shown in Figure A-2) was found to be linear and only slightly sensitive to temperature of injectate.

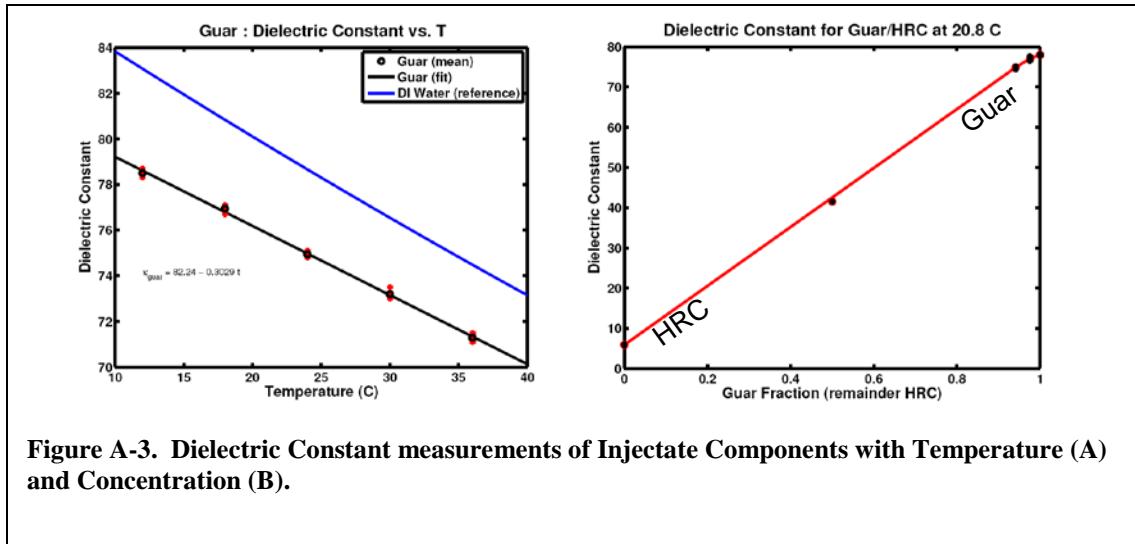


Figure A-3. Dielectric Constant measurements of Injectate Components with Temperature (A) and Concentration (B).

Dielectric Constant

Batch measurements of the dielectric constant of both the pure liquid phases (HRC & guar) as well as mixtures were obtained through use of a closed TDR cell. The resulting observations suggested that the dielectric of the initial proppant/guar should be similar to saturated formation, and that the dielectric should decrease upon injection of the HRC[®] and should decrease further as it cools after injection (Figure A-3) although temperature is unlikely to be the dominant variable. Although the dielectric signature of the injectate components were distinguishable in the laboratory, radar methods were not used during the pilot study due to high formation attenuation observe at the field site.

Laboratory Insights to Guide Field Test Design

The laboratory experiments led to the following expectations with respect to the geophysical responses to different phases of the dynamic field test:

1. Replacement of groundwater-saturated formation with proppant (e.g., sand) and guar:
 - Decrease in seismic velocity
 - Increase in electrical conductivity
 - Minimal change in dielectric constant unless gasses evolve (injection processes, calcite dissolution, guar dissolution)
2. Replacement of proppant and guar with HRC[®]:
 - Further increase in electrical conductivity
 - Increase in seismic velocity
 - Significant decrease in dielectric constant
3. HRC[®] replacement of groundwater in matrix surrounding fractures:
 - Increase in electrical conductivity
 - Decrease in dielectric constant

This information has been used in the design of the study as described in Section 5 of the Demonstration Plan.

APPENDIX B
GEOPHYSICAL WELL COORDINATES

APPENDIX B – GEOPHYSICAL WELL COORDINATES

Table B-1. Geophysical Well Coordinates

Well Name	Northing (feet)	Easting (feet)	Elevation (feet)
LBNL-1-M	231468.558	739537.334	6169.88
LBNL-2-M	231481.463	739546.901	6169.73
LBNL-3-M	231509.484	739546.402	6169.50
LBNL-4-M	231520.127	739574.092	6169.13
LBNL-5-M	231490.014	739573.708	6169.41
LBNL-6-M	231456.940	739529.044	6170.06
ERT-1	231471.543	739539.832	6170.52
ERT-2	231493.529	739555.629	6170.28
ERT-3	231506.538	739546.876	6170.20
ERT-4	231516.375	739572.003	6169.86
ERT-5	231489.612	739570.790	6170.19
F2 (Frac Well)	231486.135	739551.605	6171.02

APPENDIX C
GROUNDWATER PERFORMANCE MONITORING

APPENDIX C – GROUNDWATER PERFORMANCE MONITORING

Table C-1. Groundwater Monitoring Field Parameters

Well	Sample Date	pH	Temperature (°C)	Sp Conductance (uS/cm)	ORP (mV)	D.O. (mg/L)	Turbidity (NTUs)	Depth to GW (ft btoc)
MW-1141S	1/18/2007	6.47	7.26	955	151.3	5.00	4.68	26.06
	6/19/2007	7.18	12.95	667	187.1	4.25	72.4	24.31
	9/19/2007	7.40	13.83	662	-50.4	4.07	1.23	22.69
	12/15/2009	7.08	10.08	874	144.1	5.28	4.31	21.40
	7/6/2010	6.80	9.82	748	-42.2	4.28	NM	17.71
	7/14/2010	6.87	9.80	768	178.8	6.30	NM	16.06
	8/25/2010	6.84	9.93	883	224.7	3.84	NM	16.97
MW-1141M	1/18/2007	6.92	10.30	820	99.5	3.06	96	26.86
	6/19/2007	7.32	12.96	562	32.9	1.75	4.11	24.41
	9/19/2007	7.48	13.87	583	-81.3	1.60	1.84	22.94
	12/7/2007	7.22	7.73	710	71.3	1.61	1.47	23.80
	6/23/2008	7.11	12.88	599	153.0	1.18	1.49	24.26
	6/17/2009	7.06	13.88	934	-82.6	1.52	0.42	21.83
	12/15/2009	6.91	9.34	801	146.3	1.45	3.8	21.81
	7/6/2010	5.25	10.53	807	-63.2	0.92	NM	17.55
	7/14/2010	7.07	10.48	848	139.1	2.90	NM	17.65
8/25/2010	7.08	10.52	908	209.2	0.39	NM	18.10	
MW-1141D	1/18/2007	7.24	8.03	303	-40.6	4.21	999	25.28
	6/19/2007	8.04	15.13	217	62.4	0.59	7.41	24.40
	9/19/2007	8.38	14.04	230	-130.9	1.75	6.12	23.20
	12/7/2007	8.16	7.65	278	205.1	0.59	2.3	23.84
	6/23/2008	7.80	13.07	222	-122.4	0.21	0.85	24.44
	6/17/2009	7.51	15.48	294	-52.7	0.74	0.63	22.00
	12/15/2009	7.50	9.25	325	121.1	1.03	2.8	21.90
	7/6/2010	2.27	10.55	187	-84.6	0.26	NM	17.95
	7/14/2010	7.36	10.43	200	-184.1	3.25	NM	18.01
8/25/2010	7.02	10.53	202	-118.6	0.21	NM	18.40	
LBNL-1-M	5/19/2010	7.21	10.39	733	150.5	2.08	NM	19.43
	7/6/2010	5.26	10.43	999	-19.6	2.18	NM	17.90
	7/14/2010	7.07	10.33	1043	152.1	4.11	NM	17.98
	8/25/2010	6.79	10.41	1082	193.4	1.61	NM	18.39
LBNL-2-M	12/15/2009	7.14	10.38	788	-221.4	0.32	45.3	22.03
	5/19/2010	7.16	10.42	824	68.1	0.59	NM	19.35
	7/6/2010	4.74	10.47	895	-59.4	3.12	NM	17.82
	7/6/2010	5.99	12.10	868	-32.6	7.08	> 1000	
	7/14/2010	7.15	10.37	898	144.8	3.29	NM	17.93
8/25/2010	6.88	10.43	916	201.6	0.84	NM	18.34	

Table C-1. Groundwater Monitoring Field Parameters

Well	Sample Date	pH	Temperature (°C)	Sp Conductance (uS/cm)	ORP (mV)	D.O. (mg/L)	Turbidity (NTUs)	Depth to GW (ft btoc)
LBNL-3-M	12/15/2009	7.36	10.36	734	-213.2	0.33	28.6	21.78
	5/19/2010	7.21	10.47	775	141.3	1.87	NM	19.09
	7/6/2010	5.18	10.55	782	-19.9	2.21	NM	17.67
	7/14/2010	7.16	10.46	809	11.5	3.43	NM	17.79
	8/25/2010	7.05	10.55	813	213.2	1.62	NM	18.21
LBNL-4-M	12/15/2009	7.79	9.98	487	-169.4	0.89	12.8	21.45
	5/19/2010	7.50	10.46	625	120.5	0.39	NM	18.87
	7/6/2010	5.09	10.64	684	-32.0	2.18	NM	17.55
	7/6/2010	5.36	21.14	701	-69.2	2.62	622	
	7/14/2010	7.17	10.41	693	-22.8	4.10	NM	17.62
	8/25/2010	7.14	10.46	733	205.4	1.83	NM	18.01
LBNL-5-M	5/19/2010	7.59	10.40	664	134.0	0.45	NM	19.21
	7/6/2010	5.07	10.65	843	-18.2	0.65	NM	17.52
	7/6/2010	5.60	14.18	814	-77.2	2.14	582	
	7/14/2010	7.24	10.39	887	135.3	2.79	NM	17.76
	8/25/2010	6.97	10.46	934	213.2	0.38	NM	18.16
LBNL-6-M	12/15/2009	7.16	10.61	774	52.1	0.20	2.7	22.18
	5/19/2010	7.08	10.35	905	152.9	0.76	NM	19.55
	7/6/2010	4.49	10.43	845	-13.9	1.22	NM	17.98
	7/14/2010	7.19	10.38	878	161.0	3.75	NM	18.12
	8/25/2010	6.79	10.41	909	181.7	1.20	NM	18.41

Notes:

Denotes that parameter was taken downhole by lowering a YSI 556 to the middle of the well screen.

- °C degrees Celsius
- ft btoc feet below top of casing
- mg/L milligrams per liter
- mV millivolts
- NM Not measured. Turbidity is not measured downhole using a YSI 556.
- NTU nephelometric turbidity units
- uS/cm micro Siemens per centimeter

Table C-2. Groundwater Monitoring Analytical Results

Well I.D.	Date	ALK, T (as CaCO ₃)	TOC	Nitrogen, Ammonia (as N)	Nitrogen, Nitrate (as N)	Sulfate (as SO ₄)	Iron, T ¹	Manganese, T ¹	TCE	1,1- DCE	cis-1,2- DCE	trans- 1,2-DCE	Vinyl Chloride	DHC Enumeration	% DHC
		mg/L	mg/L	mg/L	mg/L	mg/L	mg/L	mg/L	mg/L	µg/L	µg/L	µg/L	µg/L	µg/L	number/L
MW-1141S	1/18/2007	310	--	--	16	59.0	0.130	0.055	36	--	0.22	<1	<1	--	--
	6/19/2007	300	--	--	16	65.0	0.710	0.038	36	--	0.17	<1	<1	--	--
	9/19/2007	300	--	--	17	67.0	0.150	0.009	45	--	0.18	0.07	<1	--	--
	12/15/2009	280	5	0.11	20	58	<0.2 U	0.006	16	<1 U	<1 U	<1 U	<1 U	--	--
MW-1141M	1/18/2007	270	--	--	11	52	2.000	0.160	1600	--	1.4	<5	<5	--	--
	6/19/2007	260	--	--	11	53	0.069	0.019	1400	--	1.3	0.41	<1	--	--
	9/19/2007	280	--	--	<1	56	0.025	0.012	1100	--	1.1	0.49	<4	--	--
	12/7/2007	260	--	--	11	52	0.033	0.008	1100	--	1.1	0.41	<4	--	--
	6/23/2008	268	--	--	11.5	59.8	<0.1	<0.01	848	--	0.62	<1	<1	--	--
	6/17/2009	270	--	--	10	56	<0.2	0.001	740	--	0.92	0.37	<1	--	--
	12/15/2009	260	2.2	0.048	10	56	<0.2 U	0.000	720	<2 U	0.77	0.3	<2 U	5.00E+03	0.002 - 0.006
MW-1141D	1/18/2007	120	--	--	0.97	14	35	1.1	15	--	<1	<1	<1	--	--
	6/19/2007	120	--	--	0.054	17	0.160	0.190	23	--	0.11	<1	0.089	--	--
	9/19/2007	120	--	--	0.047	15	0.032	0.200	18	--	0.12	<1	0.13	--	--
	12/7/2007	130	--	--	7.1	17	0.030	0.200	8.6	--	<1	<1	<1	--	--
	6/23/2008	132	--	--	<0.6	17.5	0.035	0.117	4.46	--	<1	<1	<1	--	--
	6/17/2009	140	--	--	0.56	15	0.023	0.010	2.1	--	<1	<1	<1	--	--
	12/15/2009	--	--	--	--	--	--	--	1.7	<1 U	<1 U	<1 U	<1 U	--	--
LBNL-2-M	12/15/2009	270	2.2	0.14	8.7	59	0.032	0.280	980	<4 U	1.1	<4 U	<4 U	2.00E+03	0.0003 - 0.0009
	7/6/2010	280	2.1	--	9	58	34	0.910	630	< 2 U	0.77 J	0.22 J	< 2 U	--	--
LBNL-3-M	12/15/2009	--	--	--	--	--	--	--	920	<4 U	<4 U	<4 U	<4 U	--	--

Table C-2. Groundwater Monitoring Analytical Results

Well I.D.	Date	ALK, T (as CaCO ₃)	TOC	Nitrogen, Ammonia (as N)	Nitrogen, Nitrate (as N)	Sulfate (as SO ₄)	Iron, T ¹	Manganese, T ¹	TCE	1,1- DCE	cis-1,2- DCE	trans- 1,2-DCE	Vinyl Chloride	DHC Enumeration	% DHC
		mg/L	mg/L	mg/L	mg/L	mg/L	mg/L	mg/L	mg/L	µg/L	µg/L	µg/L	µg/L	µg/L	number/L
LBNL-4-M	12/15/2009	--	--	--	--	--	--	--	690	0.22	0.81	<2 U	<2 U	--	--
	7/6/2010	230	1.5	--	9.9	41.0	7.9	0.210	860	< 4 U	0.56 J	< 4 U	< 4 U	--	--
LBNL-5-M	7/6/2010	260	3.2	--	8.3	62.0	10.0	0.570	690	< 2 U	0.78 J	0.19 J	< 2 U	--	--
LBNL-6-M	12/15/2009	240	2.4	0.051	7.7	57.0	<0.2 U	0.140	640	<2 U	0.73	0.23	<2 U	--	--

Notes:

-- = Not analyzed

¹Results for dissolved fraction are presented in *italics*.

APPENDIX D
SOIL BORING OBSERVATIONS

APPENDIX D – SOIL BORING OBSERVATIONS

0-1. 2011 Confirmation Soil Boring Observations

Boring ID	Date Collected	Measurement on Soil Core (feet)	Actual Depth (ft bgs)	Description	Notes
11-SB02	4/25/2011	0 - 9'	0-9'	Not logged; good sand transition to light brown; well sorted	
11-SB02	4/25/2011			Poorly sorted sand; dry chalky with gravel	
11-SB02	4/25/2011	19'	19'	Cobbles; poor recovery; clays	
11-SB02	4/25/2011	24 - 29'	24'-29'	Approx. 30% recovery; bottom 10" sandstone; approx. 50% recovery throughout	
11-SB02	4/25/2011	29-34'		Hit water at 34ft; 37" recovered; wet at top approx. 6"	
			29-31'	0-12" cookies of very cemented clays with breaks	
			31'	12", clayey and no break marks	
11-SB02	4/25/2011	34-39'		100% recovery	Reddish striations approx. 29"-32" - N Appears to be natural although could be residual HRC. No sand granules present complete (WORD) just pockets almost partially cemented (chert?) but reddish white.
			34'	0-10" very stiff clay	
			34'-36'	10-24" stiff clay with some breaks	
			36'	24-28" sandy clay with some larger grained pieces	
			36'4"	28" dry to very mushy clayey silty zone approx. 2" thick	
			36'5"-36'8"	29-32" clayey with red layer at 31.5"	
			36'9"-37'3"	33-39" more white very hard more sand fine-grained sand with silts, black/grey fractures horizontal between 34 and 38"	
			39'3"-39'6"	39-42" dry cemented	
			36'7"-38'5"	43-53" very clayey	
			38'5"-38'9"	53-57" dry chalky cookies white/grey	
38'9"-39'	57-60" cookies but more moist darker brown				
11-SB02	4/25/2011	39-44'		100% Recovery	Initiated fracture 1 at 38' bgs
			39'3"	0-3" wet white buff colored	
			39'3"-39'5"	3-5" partially cemented clayey crumbles	
			39'6"-39'10"	6-10" crumbly with more fine to med sand	
			39'10"-40'4"	10-16" sandier	
			40'5"-40'11"	17-23" cemented friable cookies	
			41'	24" blackish green approx. 1mm thick, very faint odor	
			41'11"-42'5"	35-41" more partial cemented like chocolate clayey, dark brown to orangish	
			42'7"-44'	43-60" progressively lighter sandy to chalky less clay at 44'	
42'7"-42'10"	*43.5-46" very cemented				

0-1. 2011 Confirmation Soil Boring Observations

Borehole ID	Date Collected	Measurement on Soil Core (feet)	Actual Depth (ft bgs)	Description	Notes
11-SB02	4/25/2011	44-49'		100% recovery	Initiated fracture 2 at 47' bgs; Natural seams varied through bottom 1ft of core; clays are less than 1mm, no sand, no odor; Clays are hard enough to pinch out - not much if any expansion of soils observed
			44'-45"	0-17" light buff to grey, drier sandy with cemented partially to well cemented with gravel breaking into cookies	
			45'6"-46'11"	18-35" highly cemented with plasticity, carvable but leaves grooves	
			46'11"-47'10"	35-46" carvable, drier, harder more cemented	
			47'10"-49'	46-60" harder but still carvable with a knife	
11-SB02	4/25/2011	49-54'	49'-54'	100% recovery; 41" switched to poorly graded river bed sand, large to med, no fines (photo)	Large nodules of chert in LBNL-2011 4/25/2011 a couple of times had yellow green coloring. Could have been yellow left over
11-SB04	4/25/2011	0-4'	0'-4'	Up to 50% recovery; Nothing clayey to very dry cemented; packed but brittle; black streaking vertical but no smell or sand	Approx. half way between LBNL-3M and LBNL-4M off centerline
11-SB04	4/25/2011	4-9'	4'-9'	Approx. 50% recovery; Core not logged.	
11-SB04	4/25/2011	9-14'	9'-14'	Approx. 50% recovery; Cobbles approx. 6" off foot/shoe of barrel; sands to packed fine grain sand	
11-SB04	4/25/2011	14-19'	14'-19'	Nothing	
11-SB04	4/25/2011	19-23'	19'-23'	On something very hard; pulled core and use center bit to get there	
11-SB04	4/25/2011	25'	25'	Stop for evening; 1.5' of cobbles	
11-SB04	4/26/2011	25-29'		44" total recovered	
			25'-26'9"	0-21" poorly sorted gravel with medium to large sand with some silts/clays, very small %	
			26'9"-27'	21-24" transition to partially to poorly cemented silt-clayey silt	
			27'-27'5"	24-29" buff colored dry clayey silt	
			27'5"-28'6"	29-42" darker brown, little more clay, more cemented but still friable	
			28'6"-28'8"	42-44" more clayey light brown	
11-SB04	4/26/2011	29-34'		100% recovery	
			29'-30'7"	0-19" soft clayey silt	
			30'7"-32'6"	19-42" stiff clayey silt, drier lighter brown;	
			32'6"-33'6"	42-54" harder	
			33'6"-34'	54-60" more friable/partially cemented, light buff colored, harder, some well cemented nuggets	

0-1. 2011 Confirmation Soil Boring Observations

Boring ID	Date Collected	Measurement on Soil Core (feet)	Actual Depth (ft bgs)	Description	Notes
11-SB04	4/26/2011	34-39'		100% recovery	Initiated fracture 1 at 38' bgs; Sand fra 20.25" and 20.5" approximately 1mm
			34'-34'11"	0-15" upon breaking core apart further upper portions had some reddish lenses approx. 1 mm also with strong odor	
			34'-35'4"	0-16" poorly to partially cemented silty clay/clayey silt	
			35'4"-37'	16-36" progressively harder, stiffer clayey silt with some partially to well cemented silt/clayey silts	
			35'8"	*At 20.25" approx. 1mm thick frac sand	
			35'8"	*At 20.5" presence of sand from fracturing, no color of pink, distinct odor, methanageus fermentation	
			36'5"-36'8"	*29-32" ODOR, when core first opened reddish pink orange similar to observed at LBLN-2011-SB02 observed	
			37'-37'2"	36-38" zone of lighter color grey with more cemented chunks, white well cemented nuggets	
			37'2"-38'7"	38-55" some odor although difficult to tell, reddish coloring nearly horizontal with some incline	
11-SB04	4/26/2011	39-44'		100% recovery	At 42'10" bgs approximately 1 inch th of odor.
			39'-41'	0-24" clayey silt, soft	
			41'-42'8"	24-44" stiff, more cemented, some well and poorly cemented lenses, some cemented nuggets	
			42'8"-43'6"	44-54" more cemented, friable	
			42'5"-42'11"	*41-47" lenses of reddish orange	
			42'10"-42'11"	*46-47" approx. 1 inch thick zone of odor	
			42'5"	*41" 1/8" thick zone	
			42'7"	*43" thinner colorations	
	*10-11" color but not much odor				
11-SB04	4/26/2011	44-49'		100% recovery	Initiated fracture 2 at 47' bgs
			44'-44'9"	0-9" colorations but no odor	
			44'9"-45'6"	9-18" sandy, rest of core partially to well cemented, brown to buff	
			45'11"-46'10"	23-34" colorations but no odor	
			46'4"-47'4"	28-41" colorations but no odor	
11-SB04	4/26/2011	49-54'		93% recovery	
			49'-49'4"	0-4" slough;	

1. 2011 Confirmation Soil Boring Observations

Core ID	Date Collected	Measurement on Soil Core (feet)	Actual Depth (ft bgs)	Description	Notes
			49'4"-49'9"	4-9" partially cemented claystone	
			49'10"-50'5"	10-17" more sandy	
			50'5"-52'3"	17-39" clayey/sandy silty	
			52'3"-53'8"	39-56" well sorted medium grained sand	
			52'5", 52'9", 52'11"	*At 41-42", 45", 47" grey/green, slight odor	
11-SB01	4/26/2011	0-19'	0'-19'	Core not logged.	
11-SB01	4/26/2011	19-24'		90% recovery, poorly to well cemented	
			19'-20'9"	0-21" clayey silt	
			20'10"-22'	22-36" sandy silt, silty sand, bit of clay	
			22'-22'11"	36-47" firm packed fine grained sand with clays/silty clay	
		22'11"-23'7"	47-55" dry silty, buff (lighter) colored		
11-SB01	4/26/2011	24-29'		95% recovery	
			24'26'9"	0-33" partially to mostly cemented silts with some fine grained sand and clay cookies	
			26'9"-28'2"	33-50" some reddish lenses, no odor, silty clay, mostly cemented crumbles	
			28'2"-28'6"	50-54" brown silty clay	
		28'6"-28'9"	54-57" buff partially cemented silt		
11-SB01	4/26/2011	29-34'		100% recovery	
			29'-32'2"	0-38" clay with fine grained sand and silts	
			32'2"-33'	38-48" much more cemented with light buff color	
			33'-33'4"	48-52" darker with large cemented cobbles	
		33'4"-34'	52-60" much less cemented clay with silts, fine grained sand		
11-SB01	4/26/2011	34-39'	34'-39'	Core not logged	Initiated fracture 1 at 38' bgs. Three samples collected here. Cut into 1.75' for shipment to LBNL. Some fracture maybe present but didn't want to disturb core, so didn't open. Sample 1 at 34'-35'8"; Sample 2 at 35'8"-37'4"; Sample 3 at 37'4"-39'
11-SB01	4/26/2011	39-44'		100% recovery	On end and inside core band very sorted likely fracture sand. Photos of top and outer side. May have hit fracture at 39'41'7" bgs, 1/8 to 1/4 inch (3.175-6.35mm) coloration, possible fracture.
			39'-39'9"	0-9" partially cemented lenses with silty sandy clay	
			39'9"-40'7"	9-19" less cemented, more fine sand and silts	
			40'6"-40'11"	18-23" brittle, friable cemented cookies	
			40'11"-42'4"	23-40" clayey silt	
		41'7"	*At 32" green grey black stripe, 1/8 to 1/4" thick across horizontal, some odor, no frac sand		

0-1. 2011 Confirmation Soil Boring Observations

Boring ID	Date Collected	Measurement on Soil Core (feet)	Actual Depth (ft bgs)	Description	Notes
			42'4"-43'2"	40-50" more sandy packed, very few cemented, some orangey colored variations, no odor	
			43'3"-44'	51-60" lighter partially to well cemented chalky/white buff	
11-SB01	4/26/2011	44-49'	44'-49'	Core not logged	Initiated fracture 2 at 47'bgs. Three soil samples collected here. Cut into 1.75' lengths. Sample 1 at 44'-45'8"; Sample 2 at 45'-46'8"; Sample 3 at 47'4"-49'
11-SB01	4/26/2011	49-54'		100% recovery	At 51'11"bgs 1/8 to 1/4 inch (3.175-6.35mm) greenish grey colorations, possible fracture
			49'-49'5"	0-5" slough with clay	
			49'5"-51'5"	5-29" silty clay partially cemented	
			51'5"-51'8"	29-32" transition from fine grained sand to medium sand	
			51'8"-52'4"	32-40" medium sand	
			51'11"	*At 35" another greenish black 1/8-1/4" thick lense with some odor, greyish yellowish	
			52'2"-52'3"	*At 38-39.5" poorly sorted	
			52'4"-54'	40-60" progressively more sand to gravel with some silt clay	
		53'-53'2"	*At 48-50" some cemented white chert with some yellow tinge, chert nodules through 45-60"		
11-SB01	4/26/2011	54-68'	54'-68'	Total depth is 68ft bgs; Core not logged	Driller aimed for 67', accidentally went 1' deeper. Well from 33-43' to cover Fracture 1 and Fracture 2 in the middle.
11-SB03	4/27/2011			Core not logged	Initiated fracture 1 at 38' bgs and fracture 2 at 47'bgs; Soil samples collected at 34'-35'8", 39'-40'8", 44'-44'9", and 49'-54'
11-SB03	4/27/2011	29-34'	29'-34'	87% recovery; Core not logged	
11-SB03	4/27/2011	34-39'	34'-39'	70% recovery; Core not logged	Sample 1 cut into 2, 21" lengths
11-SB03	4/27/2011	39-44'	39'-44'	100% recovered; Core not logged	Sample 2 cut into 20" sections
11-SB03	4/27/2011	44-49'	44'-49'	100% recovered, a lot of slough at approx. 6" of core; Core not logged	
11-SB03	4/27/2011	49-54'	49'-54'	87% recovery; approx. 52" of 60" core collected; 44.5" of total sands out of core sleeve in core barrel; 0-20", 20-40", 40-44.5"; Core not logged	

Notes:

ft bgs = feet below ground surface

APPENDIX E
DESCRIPTION OF S-WAVE SOURCE EXPERIMENTS

As discussed in the demonstration plan, LBNL fielded a newly developed high-speed orbital vibrator (HSOV) source as part of the WAFB fracture characterization pilot to enable timelapse acquisition of both P and S wave seismic imagery. This selection was motivated by theoretical and laboratory studies which suggested that S wave measurements may provide a better indicator of fracture properties. The HSOV was descended from a similar orbital source originally developed by Conoco but modified for the higher frequencies and smaller wells diameters more relevant to environmental sites.

During the site reconnaissance trip conducted early in the project, the HSOV source was field tested and demonstrated capable of generating measurable seismic signals at significant offsets (over 100 ft); however, the initial reconnaissance measurements were not quantitatively processed because of the significant required effort and low relevance to the final pilot. As part of the pilot fracture deployment, the HSOV was used to acquire multiple crosswell surveys both before and after the fracture installation. Well 6M, the one borehole capable of accommodating the source, was used as the source well and surveys were shot into a 48-level hydrophone array sequentially deployed in wells 1M, 2M, 3M, 4M, and 5M. Like the reconnaissance surveys, the raw data acquired appeared to have a high signal-to-noise (S/N) level but could not be interpreted in the field due to several time-consuming processing steps which had to be conducted off-line.

After the pilot fracture surveys were completed, a comprehensive processing effort was initiated to evaluate the HSOV dataset. The processing flow included various format conversions, deconvolution, designaturing, and component rotation. An identical processing flow had been successfully applied to prior studies using a previous OV source. However, the interpretability of the processed data was poor; no S-wave arrivals were visible in the final gathers and the P-wave signal, while visible with excellent S/N levels, did not have the proper kinematic characteristics. Both issues limited the use of the HSOV timelapse dataset in understanding fracture propagation at the WAFB pilot and the problem remained a mystery for several months.

Subsequently, while pre-testing the HSOV system for possible future surveys, the source of the poor interpretability was identified. The HSOV source, unlike prior OV sources, had a soft cable to allow easy deployment by a single operator in shallow wells rather than a stiff 7-conductor cable more typical of petroleum wireline operations; unfortunately, this softer cable resulted in the source changing orientation during operation in an unpredictable fashion due to the torque applied during motor operation. The processing flow developed previously requires the orientation of the source to remain constant during a single sweep, hence the poor interpretability of the final gathers despite the excellent S/N in raw gathers. This design issue will be corrected in future deployments but cannot be retroactively accommodated with the analysis methods we have used.

In conclusion, the HSOV source was tested and then deployed as part of our Warren AFB fracture monitoring pilot. The timelapse surveys effectively demonstrated the potential of orbital source technologies and the HSOV source was visible at offsets where our existing piezoelectric source could not be recorded. However, a design flaw in the cable prevented the LBNL team from effectively analyzing the acquired datasets. Our

findings do not reflect negatively on the utility of S-waves for fracture monitoring but do demonstrate that the HSOV system will required further refinement before it is suitable for routine field deployment at such sites.

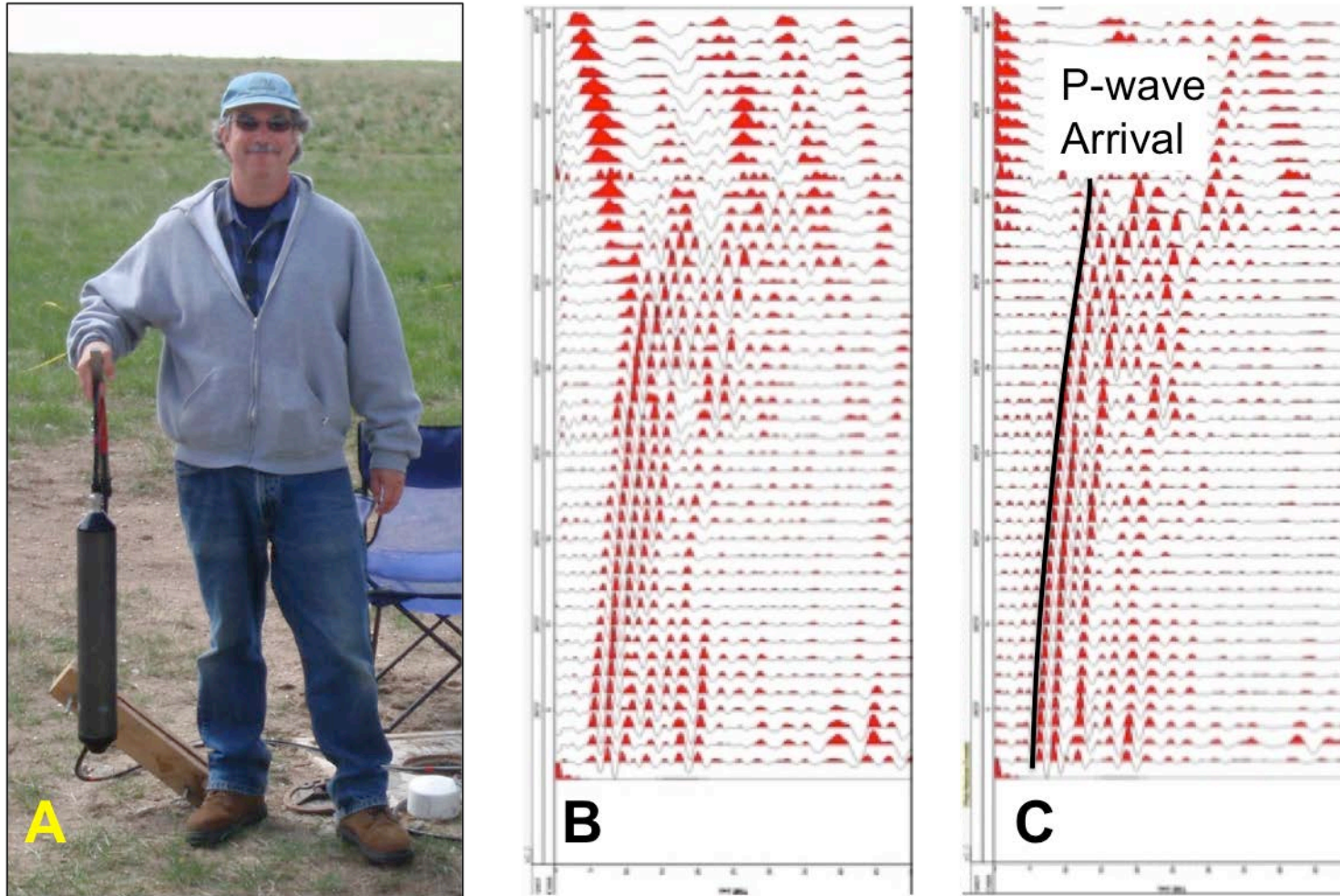


Figure 22 : HSOV source and example gathers : Panel A shows the high-speed orbital vibrator source as deployed on a flexible two-component cable (w. T. Daley). Panels B and C show example gathers after designating but before and after component rotation respectively. As can be seen in panel C, the direct P arrival is quite strong but no direct S-arrival is visible.